Macrophages regulate gastrointestinal motility through complement component 1q

Mihir Pendse[1], Yun Li[1], Cristine N. Salinas[1], Gabriella Quinn[1], Nguyen Vo[1], Daniel C. Propheter[1], Chaitanya Dende[1], Alexander A. Crofts[1], Eugene Koo[1], Brian Hassell[1], Kelly A. Ruhn[1], Prithvi Raj[1], Yuuki Obata[1*], Lora V. Hooper[1,2*]

[1]Department of Immunology, The University of Texas Southwestern Medical Center, Dallas, TX 75390

[2]The Howard Hughes Medical Institute, The University of Texas Southwestern Medical Center, Dallas, TX 75390

***For correspondence:** yuuki.obata@utsouthwestern (YO), lora.hooper@utsouthwestern.edu (LVH)

ABSTRACT

Peristaltic movement of the intestine propels food down the length of the gastrointestinal tract to promote nutrient absorption. Interactions between intestinal macrophages and the enteric nervous system regulate gastrointestinal motility, yet we have an incomplete understanding of the molecular mediators of this crosstalk. Here we identify complement component 1q (C1q) as a macrophage product that regulates gut motility. Macrophages were the predominant source of C1q in the mouse intestine and most extraintestinal tissues. Although C1q mediates complement-mediated killing of bacteria in the bloodstream, we found that C1q was not essential for immune defense of the intestine. Instead, C1q-expressing macrophages were localized to the intestinal submucosal plexus where they were closely associated with enteric neurons and expressed surface markers characteristic of nerve-adjacent macrophages in other tissues. Mice with a macrophage-specific deletion of *C1qa* showed changes in enteric neuronal gene expression, increased peristaltic activity, and accelerated intestinal transit. Our findings identify C1q as a key regulator of gastrointestinal motility and provide enhanced insight into the crosstalk between macrophages and the enteric nervous system.

INTRODUCTION

Peristalsis is the physical force that propels food through the intestine, promoting digestion and nutrient absorption. The gastrointestinal motility that underlies peristalsis is a complex process that requires coordination of the activity of smooth muscle cells by enteric neurons (Rao and Gershon, 2016). Recent studies have revealed that intestinal macrophages impact gastrointestinal motility by regulating the functions of enteric neurons and facilitating their interactions with smooth muscle cells (Muller et al., 2014; Matheis et al., 2020).

Macrophages carry out diverse functions in the intestine that vary according to their anatomic location. For example, macrophages that localize to the tissue located directly underneath the gut epithelium — known as the lamina propria — contribute to immune defense against pathogenic bacteria

27 (Gabanyi et al., 2016). A distinct group of macrophages localizes to the tissues located beneath the lamina
28 propria, between the circular and longitudinal muscle layers in the tissue region known as the muscularis
29 externa. These muscularis macrophages express genes that are distinct from lamina propria macrophages
30 (Gabanyi et al., 2016). They directly regulate the activity of smooth muscle cells (Luo et al., 2018) and
31 secrete soluble factors such as bone morphogenetic protein 2 (BMP2) that interact with the enteric neurons
32 that control smooth muscle activity (Muller et al., 2014). Muscularis macrophages thus play a key role in
33 regulating gut motility. However, our understanding of the molecular mechanisms by which these
34 macrophages regulate intestinal neuromuscular activity and gut motility remains limited.

35 C1q is a member of the defense collagen family that has distinct functions in immune defense and
36 nervous system development and function (Bossi et al., 2014; Casals et al., 2019; Shah et al., 2015; Thielens
37 et al., 2017). C1q is composed of six molecules each of C1qA, C1qB, and C1qC, forming a 410 kDa
38 oligomer. C1q circulates in the bloodstream, where it participates in immune defense against infection by
39 recognizing antibodies bound to invading bacteria. This binding interaction initiates the classical
40 complement pathway, which entails the recruitment and proteolytic processing of other complement
41 components that rupture the bacterial membrane and recruit phagocytic cells (Kishore and Reid, 2000;
42 Noris and Remuzzi, 2013). C1q is also produced by microglia (brain-resident macrophage-like cells) in the
43 brain where it promotes the pruning of neuronal synapses through an unclear mechanism (Hammond et al.,
44 2020; Hong et al., 2016). Consequently, C1q deficiency results in heightened synaptic connectivity in the
45 central nervous system that can lead to epilepsy (Chu et al., 2010).

46 C1q is also produced at barrier sites, such as the intestine, where encounters with commensal and
47 pathogenic microbes are frequent. However, little is known about the physiological role of C1q in barrier
48 tissues. Liver immune cells, including macrophages and dendritic cells, produce serum C1q; however the
49 cellular source of C1q in barrier tissues including the intestine remains unclear (Petry et al., 2001). Here,
50 we show that C1q is selectively produced by macrophages that inhabit the submucosal plexus of the mouse
51 intestine. These C1q-expressing macrophages are located close to enteric neurons that have a known role
52 in controlling gut motility. Consistent with their nerve-adjacent localization, mice lacking macrophage C1q

53 exhibit altered expression of enteric neuronal genes, increased peristaltic activity, and accelerated
54 gastrointestinal motility. These findings identify C1q as a key mediator of a neuroimmune interaction that
55 regulates gut motility.
56
57
58 **RESULTS**
59 **C1q is expressed in intestinal macrophages**
60 Soluble defense collagens are an ancient, evolutionarily conserved family of antimicrobial proteins
61 with shared structural features including a *C*-terminal globular head and a collagen-like region (Casals et
62 al., 2019). Little is known about the function of defense collagens at mucosal barrier sites, where microbial
63 encounter is frequent. Our initial goal in this study was to identify soluble defense collagens that are
64 expressed by the mouse intestine and to assess their role in host defense. We therefore measured the
65 expression of 18 defense collagen genes in the mouse small intestine and colon by RNA sequencing (RNA-
66 seq). This analysis revealed that the most abundant soluble defense collagen transcripts in the small intestine
67 and colon were those encoding C1qA, C1qB, and C1qC (***Figure 1A; Figure 1 – figure supplement 1***).
68 Serum C1q is produced by liver dendritic cells, monocytes, and macrophages (El-Shamy et al.,
69 2018). However, the cellular source(s) of C1q in peripheral tissues including the intestine is unknown.
70 Quantitative PCR (qPCR) analysis of fluorescence-activated cell sorting (FACS)-sorted cell suspensions
71 recovered from the small intestines of wild-type C57BL/6 mice revealed that *C1qa*, *C1qb*, and *C1qc*
72 transcripts were most abundant in $CD45^+$ cells, which include all immune cells, as compared to $CD45^-$ cells,
73 which encompass non-immune cells such as epithelial cells (***Figure 1B***). Further, C1q transcripts and
74 protein were most abundant in $CD45^+$ cells recovered from the subepithelial compartment, which includes
75 both the lamina propria and muscularis, as compared to $CD45^+$ cells recovered from the intraepithelial
76 compartment of the small intestine (***Figure 1C and D***). Thus, C1q is expressed by immune cells located in
77 the subepithelial compartment of the intestine and is largely absent from epithelial cells and intraepithelial
78 immune cells.

To identify the intestinal immune cell population that expresses C1q, we further analyzed the subepithelial CD45^{+} cell population by flow cytometry. Expression of C1q transcripts and protein was highest in CD11b^{+}MHCII^{+}F4/80^{hi} macrophages and was mostly absent from all non-macrophage immune cells (***Figure 1E-H***). Thus, C1q is expressed by macrophages in the mouse small intestine.

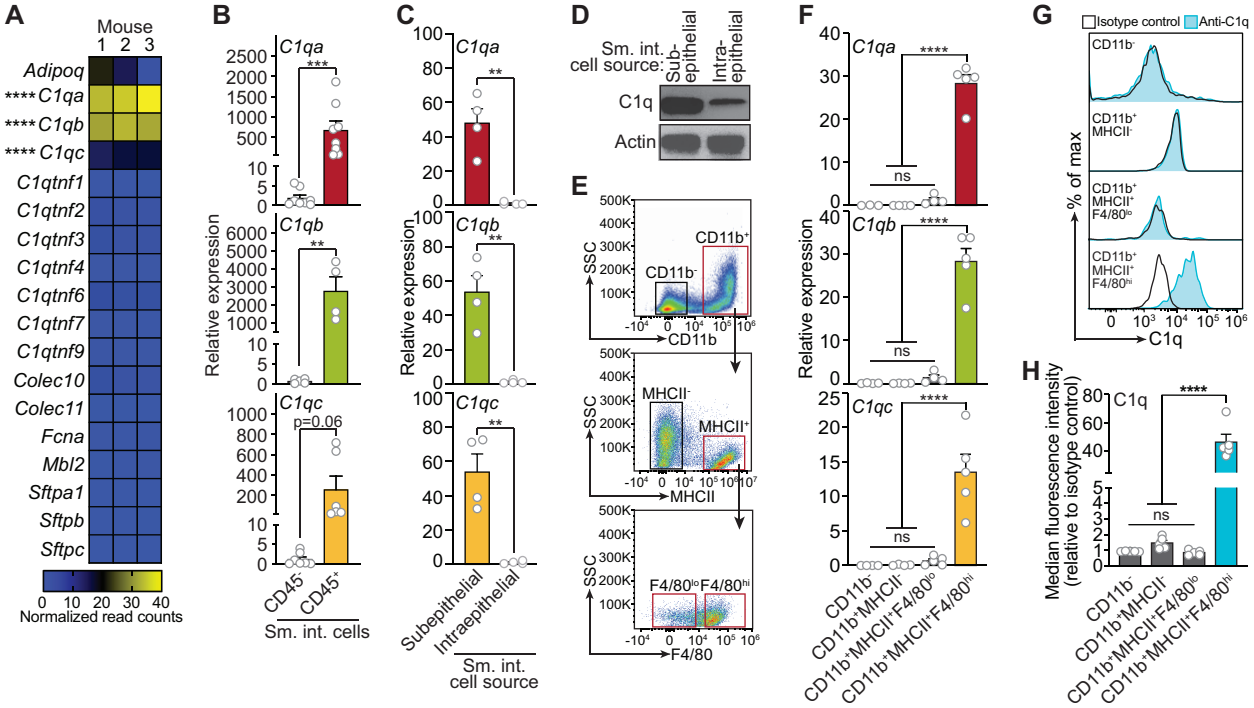

Figure 1. C1q is expressed by macrophages in the mouse small intestine.
(A) RNA-seq analysis of soluble defense collagen expression in the small intestines (ileum) of C57BL/6 mice. Data were adapted from a previously published RNA-seq analysis (Gattu et al., 2019). Data are available in the Gene Expression Omnibus repository under accession number GSE122471. Each column represents one mouse.
(B) qPCR measurement of *C1qa*, *C1qb*, and *C1qc* transcript abundance in CD45^{+} and CD45^{-} cells purified from mouse small intestines by flow cytometry. Each data point represents one mouse, and results are representative of two independent experiments.
(C) qPCR measurement of *C1qa*, *C1qb*, and *C1qc* transcript abundance in subepithelial and intraepithelial cells recovered from mouse small intestines. Each data point represents one mouse, and results are representative of three independent experiments.
(D) Representative immunoblot of subepithelial and intraepithelial cells recovered from mouse small intestines, with detection of C1q and actin (control). Each lane represents cells from one mouse and immunoblot is representative of three independent experiments.
(E) Flow cytometry gating strategy for analysis of mouse small intestinal cell suspensions in panels F, G, and H. Cells were pre-gated as live CD45^{+} cells. SSC, side-scatter; MHCII, major histocompatibility complex II.
(F) qPCR measurement of *C1qa*, *C1qb*, and *C1qc* transcript abundance in cells isolated by flow cytometry from mouse small intestines as indicated in (E). Each data point represents cells pooled from three mice, and results are representative of three independent experiments.
(G) Flow cytometry analysis of intracellular C1q in small intestinal subepithelial cells identified as indicated in (E).
(H) Quantitation of flow cytometry analysis in (G). Each data point represents one mouse, and results are representative of two independent experiments.

Sm. int., mouse small intestine; Error bars represent SEM. **p<0.01; ***p<0.001; ****p<0.0001; ns, not significant by one way ANOVA (A,F) or two-tailed Student's t-test (B,C,H).

Figure supplement 1. C1q is expressed in the mouse colon.

Macrophages are the primary source of C1q in the mouse gastrointestinal tract

We next assessed whether macrophages are the primary source of C1q in the intestine by analyzing two mouse models. First, we depleted macrophages by injecting neutralizing antibodies directed against the receptor for colony stimulating factor 1 (CSF1R)(***Figure 2A***), which is required for the development of a subset of lamina propria macrophages (Bogunovic et al., 2009) and all muscularis macrophages (Muller et al., 2014). Antibody injection led to a >2-fold reduction in the number of macrophages recovered from the small intestine (***Figure 2B***), and a corresponding >2-fold reduction in small intestinal C1q gene expression **(*Figure 2C*)**, suggesting that macrophages are the primary source of intestinal C1q.

Second, we constructed a genetic model of C1q deficiency by crossing *C1qa*$^{fl/fl}$ mice (Fonseca et al., 2017) to mice carrying the *Lyz2-Cre* transgene (LysM-Cre mice), which is selectively expressed in myeloid cells including macrophages (***Figure 2D***). These mice, hereafter designated as *C1qa*$^{\Delta M\phi}$ mice, lacked C1q expression in intestinal macrophages (***Figure 2E and F***). Importantly, *C1qa*$^{\Delta M\phi}$ mice had markedly lower overall C1q expression in both the small intestine and colon (***Figure 2G***), indicating that macrophages are the main source of C1q in the intestine. Unexpectedly, the *C1qa*$^{\Delta M\phi}$ mice also lost *C1q* gene expression in the lung, skin, kidney, and liver (but not the brain), and C1q protein was undetectable in the serum (***Figure 2 – figure supplement 1***). These findings indicate that macrophages are the primary source of C1q in the intestine and suggest that LysM^{+} macrophages or macrophage-like cells are also the main source of C1q in most extraintestinal tissues and the bloodstream.

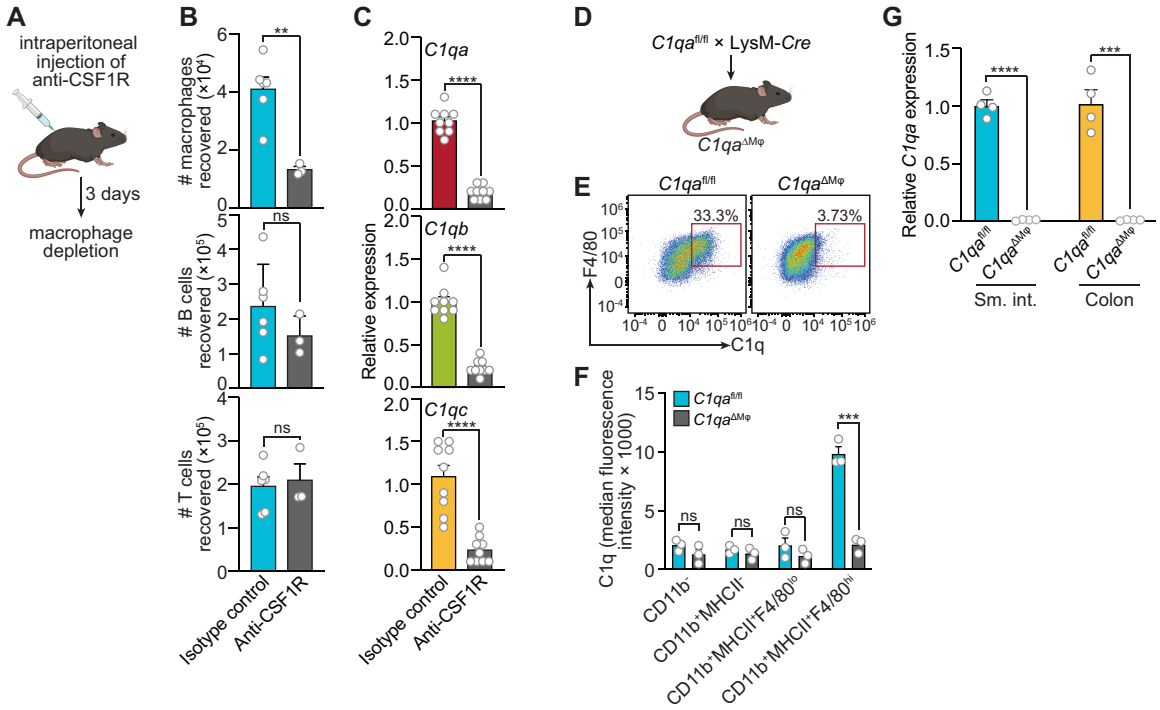

Figure 2. Macrophages are the primary source of C1q in the mouse gastrointestinal tract.
(A) Graphic showing selective depletion of macrophages in C57BL/6 mice by intraperitoneal injection of anti-CSF1R antibody. Control mice were injected with isotype-matched non-specific antibody. Mice were analyzed 72 hours after antibody injection. Panel was generated at Biorender.com.
(B) Representative flow cytometry analysis of mouse small intestines after intraperitoneal injection of anti-CSF1R or isotype control antibody. All cells were gated as live $CD45^+$. Macrophages were $MHCII^+$ $F4/80^{hi}$; B cells were $CD19^+$; T cells were $CD3^+$. Total small intestinal cell yields were $1.5 \times 10^6 \pm 4.9 \times 10^5$ cells.
(C) qPCR measurement of *C1qa*, *C1qb*, and *C1qc* transcript abundance in mouse small intestines after intraperitoneal injection of anti-CSF1R or rat IgG2a (isotype control). Each data point represents one mouse and results are pooled from two independent experiments.
(D) $C1qa^{fl/fl}$ mice were crossed with mice harboring a LysM-Cre transgene to generate mice having a macrophage-selective deletion of *C1qa* ($C1qa^{\Delta M\varphi}$ mice). Panel was generated at Biorender.com.
(E) Representative flow cytometry analysis of intracellular C1q expression in small intestinal macrophages from $C1qa^{fl/fl}$ and $C1qa^{\Delta M\varphi}$ mice. Mice were littermates from heterozygous crosses that remained co-housed. Cells were gated on live $CD45^+CD11b^+MHCII^+$.
(F) Quantitation of the flow cytometry analysis in (E). Each data point represents one mouse. Results are representative of two independent experiments.
(G) qPCR measurement of *C1qa* transcript abundance in the small intestines (sm. int.) and colons of $C1qa^{fl/fl}$ and $C1qa^{\Delta M\varphi}$ littermates. Each data point represents one mouse.

Error bars represent SEM. **p<0.01; ***p<0.001; ****p<0.0001; ns, not significant by two-tailed Student's t-test.

Figure supplement 1. C1q expression is lost systemically but preserved in the central nervous system of $C1qa^{\Delta M\varphi}$ mice.

158 ***C1qa*$^{\Delta M\varphi}$ mice do not show altered microbiota composition, barrier function, or resistance to enteric**
159 **infection**

160 The classical complement pathway is a well-studied host defense system that protects against
161 systemic pathogenic infection (Warren et al., 2002; Noris and Remuzzi, 2013). Circulating C1q activates
162 the complement pathway by binding to antibody-antigen complexes or to bacterial cell surface molecules,
163 and thus protects against systemic infection. We therefore assessed whether C1q promotes immune defense
164 of the intestine.

165 We first determined whether C1q exhibits characteristics of known intestinal antimicrobial
166 proteins, including induction by the intestinal microbiota and secretion into the gut lumen. *C1qa* was
167 expressed at similar levels in the small intestines of germ-free and conventionally-raised mice (***Figure 3A***),
168 suggesting that *C1q* expression is not induced by the gut microbiota. This contrasted with *Reg3g*, encoding
169 the antimicrobial protein REG3G (Cash et al., 2006), which was expressed at a >2-fold higher level in
170 conventional as compared to germ-free mice (***Figure 3A***). Additionally, in contrast to REG3G, C1q was
171 not detected in the gut lumen of either conventional or germ-free mice (***Figure 3B***). *C1qa* expression was
172 also not markedly altered by oral infection with the intestinal pathogenic bacterial species *Salmonella*
173 Typhimurium (***Figure 3C***). These data indicate that C1q is not induced by the gut microbiota or by the
174 bacterial pathogen *S.* Typhimurium, in contrast to other antibacterial proteins.

175 We next assessed whether C1q regulates the composition of the gut microbiota. 16*S* rRNA gene
176 sequencing analysis of the fecal microbiotas of *C1qa*$^{fl/fl}$ and *C1qa*$^{\Delta M\phi}$ mice showed that the microbiota
177 composition was not appreciably altered in the absence of macrophage C1q (***Figure 3D***). We also
178 challenged *C1qa*$^{fl/fl}$ and *C1qa*$^{\Delta M\phi}$ mice with dextran sulfate sodium (DSS), which damages the colonic
179 epithelium and exposes underlying tissues to the commensal microbiota. However, the sensitivity of the
180 *C1qa*$^{\Delta M\phi}$ mice to DSS was similar to that of their *C1qa*$^{fl/fl}$ littermates as assessed by change in body weight
181 (***Figure 3E***). There was also no change in intestinal paracellular permeability in *C1qa*$^{\Delta M\phi}$ mice as measured

182 by oral administration of FITC-dextran (***Figure 3F***). These results suggest that macrophage C1q does not
183 substantially impact gut microbiota composition or intestinal epithelial barrier function.

184 To determine whether C1q protects against enteric infection we conducted oral infection
185 experiments with the enteric pathogen *Citrobacter rodentium*. We chose *C. rodentium* as our model
186 organism for two reasons. First, *C. rodentium* is a non-disseminating pathogen, allowing us to test
187 specifically for C1q's role in intestinal infection. Second, *C. rodentium* clearance depends on
188 immunoglobulins and complement component C3 (Belzer et al., 2011). Because C1q is bactericidal in
189 concert with C3 and immunoglobulins, we predicted that $C1qa^{\Delta M\phi}$ mice would show enhanced
190 susceptibility to *C. rodentium* infection. However, $C1qa^{\Delta M\phi}$ mice cleared *C. rodentium* similarly to their
191 $C1qa^{fl/fl}$ littermates, indicating that C1q is dispensable for defense against *C. rodentium* infection (***Figure***
192 ***3G***).

193 We also did not observe marked alterations in immunity in the absence of C1q. Comparison of
194 cytokine transcript abundance in the small intestines of $C1qa^{fl/fl}$ and $C1qa^{\Delta M\phi}$ littermates revealed no
195 statistically significant differences in cytokine expression (***Figure 3H***). There were also no statistically
196 significant differences in the percentages or absolute numbers of various T cell subsets, including $T_{helper}1$
197 (T_H1), T_H2, T_H17, and regulatory T (T_{reg}) cells between $C1qa^{fl/fl}$ and $C1qa^{\Delta M\phi}$ mice (***Figure 3I; Figure 3 –***
198 ***figure supplement 1***). Although total B cell numbers trended lower in $C1qa^{\Delta M\phi}$ mice, the difference was
199 not statistically significant (***Figure 3I; Figure 3 – figure supplement 2***). There were also no statistically
200 significant differences in the percentages or absolute numbers of total plasma cells (***Figure 3I; Figure 3 –***
201 ***figure supplement 2***), IgA^+ plasma cells (***Figure 3I; Figure 3 – figure supplement 2***), myeloid cells
202 (***Figure 3I; Figure 3 – figure supplement 3***), or innate lymphoid cells (***Figure 3I; Figure 3 – figure***
203 ***supplement 4***) when comparing $C1qa^{fl/fl}$ and $C1qa^{\Delta M\phi}$ mice. These results suggest that the absence of
204 macrophage C1q has little impact on intestinal immunity. Altogether, our findings suggest that C1q does
205 not participate substantially in intestinal immune defense and thus might have an intestinal function that is
206 independent of its canonical role in activating the classical complement pathway.

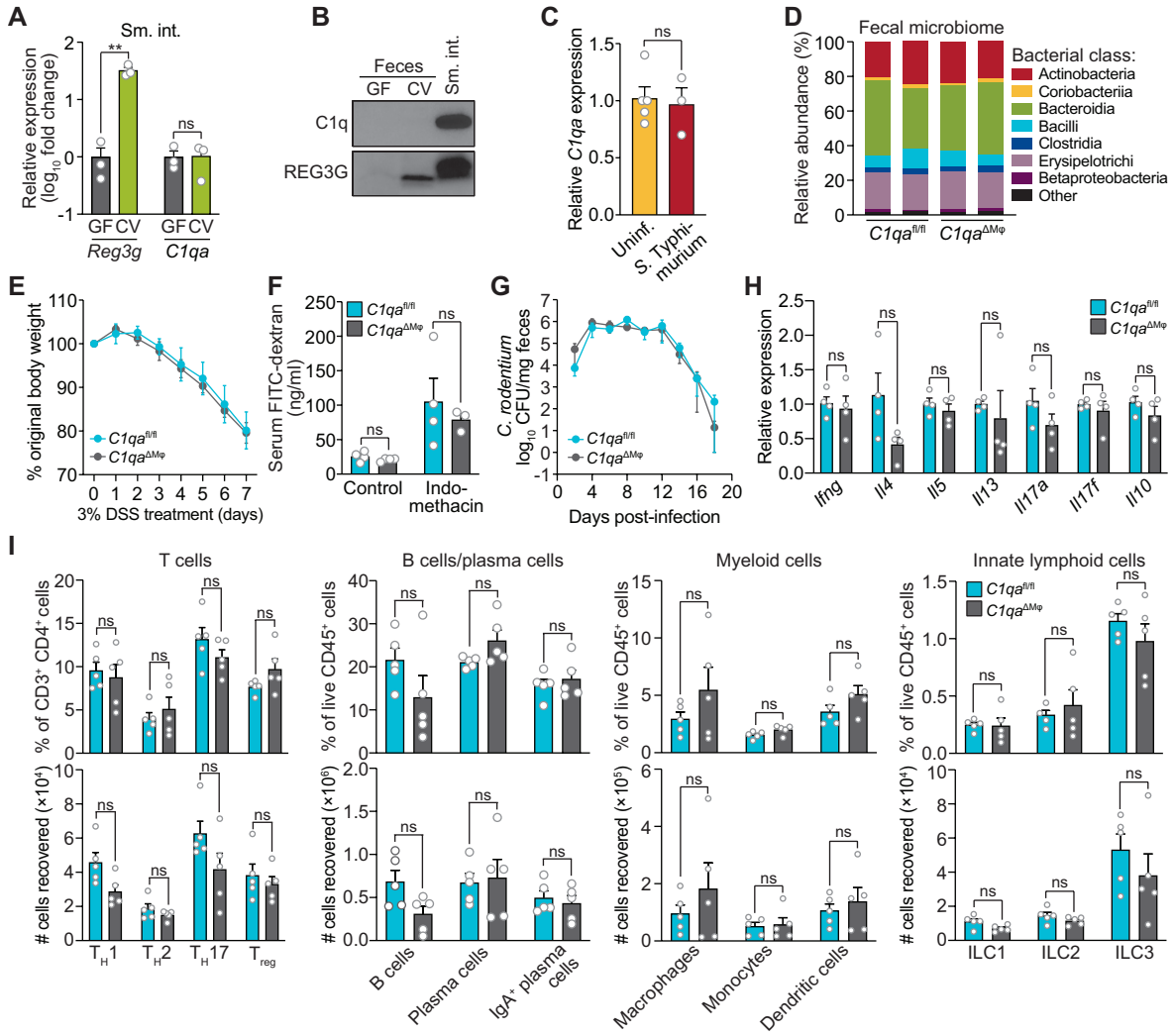

Figure 3. *C1qa*$^{\Delta M\varphi}$ mice do not show altered microbiota composition, barrier function, or resistance to enteric infection.

(A) Small intestinal *C1qa* expression is not induced by the intestinal microbiota. qPCR measurement of *Reg3g* and *C1qa* transcript abundances in the small intestines of germ free (GF) and conventional (CV) C57BL/6 mice. Each data point represents one mouse and results are representative of two independent experiments.

(B) C1q is not detected in the mouse intestinal lumen or feces. Representative immunoblot of an ammonium sulfate precipitation of intestinal lumenal contents and feces from germ-free and conventional mice with detection of C1q. C1q in small intestinal tissue (sm. int.) is shown for comparison at right. REG3G was detected as a control, as it is secreted into the intestinal lumen of conventional mice (Cash et al., 2006). Each lane represents multiple mice pooled (n = 5 and 9 for germ-free and conventional, respectively) and the immunoblot is representative of three independent experiments.

(C) C1q gene expression is not altered by enteric infection with *S.* Typhimurium. qPCR measurement of *C1qa* transcript abundance in small intestinal tissue after oral inoculation of mice with 10^9 colony forming units of *S.* Typhimurium strain SL1344. Each data point represents one mouse, and results are representative of two independent experiments.

(D) Intestinal microbiota composition is not altered in *C1qa*$^{\Delta M\varphi}$ mice. Phylogenetic analysis of 16*S* rRNA gene sequences from fecal pellets collected from *C1qa*$^{fl/fl}$ and *C1qa*$^{\Delta M\varphi}$ littermates. Operational taxonomic units with an

225 average of 100 reads and populations greater than or equal to 1% were included in the graphical analysis. Each bar
226 represents one mouse. Data are available from the Sequence Read Archive under BioProject ID PRJNA793870.
227 **(E)** *C1qa*$^{\Delta M\varphi}$ mice do not show altered susceptibility to dextran sulfate sodium (DSS)-induced colitis. Mice were
228 provided with 3% DSS in drinking water and body weights were monitored for 7 days. n = 4 and 6 for *C1qa*$^{fl/fl}$ and
229 *C1qa*$^{\Delta M\varphi}$ littermates, respectively. Error bars represent SEM. Differences at each time point were not significant by
230 two-tailed Student's t-test.
231 **(F)** *C1qa*$^{\Delta M\varphi}$ mice do not show altered intestinal permeability. To measure intestinal permeability, *C1qa*$^{fl/fl}$ and
232 *C1qa*$^{\Delta M\varphi}$ littermates were gavaged with FITC-dextran, and serum FITC-dextran levels were determined by
233 fluorescence microplate assay against a FITC-dextran standard curve. Indomethacin induces intestinal damage in mice
234 and was used as a positive control.
235 **(G)** Time course of fecal *C. rodentium* burden following oral gavage of *C1qa*$^{fl/fl}$ and *C1qa*$^{\Delta M\varphi}$ mice with 5×10^8 colony
236 forming units (CFU) of *C. rodentium*. n = 5 and 5 for *C1qa*$^{fl/fl}$ and $^{C1qa\Delta M\varphi}$ littermates, respectively. Error bars represent
237 SEM. Differences at each time point were not significant by two-tailed Student's t-test.
238 **(H)** qPCR measurement of cytokine transcript abundances in the small intestines of *C1qa*$^{fl/fl}$ and *C1qa*$^{\Delta M\varphi}$ littermates.
239 Error bars represent SEM. Statistics were performed with two-tailed Student's t-test.
240 **(I)** Flow cytometry analysis of small intestinal immune cell subsets from *C1qa*$^{fl/fl}$ and *C1qa*$^{\Delta M\varphi}$ littermates. Gating
241 strategies are shown in Figure 3 - figure supplement 1 through 4. ILC, innate lymphoid cell. Total small intestinal cell
242 yields were $8.8 \times 10^6 \pm 2.9 \times 10^6$ cells.
243
244 Error bars represent SEM. **p<0.01; ns, not significant by two-tailed Student's t-test.
245
246 **Figure supplement 1.** Flow cytometry gating strategy for comparison of T cell populations in *C1qa*$^{fl/fl}$ and *C1qa*$^{\Delta M\varphi}$
247 mice.
248 **Figure supplement 2.** Flow cytometry gating strategy for comparison of B cell and plasma cell populations in *C1qa*$^{fl/fl}$
249 and *C1qa*$^{\Delta M\varphi}$ mice.
250 **Figure supplement 3.** Flow cytometry gating strategy for comparison of myeloid cell populations in *C1qa*$^{fl/fl}$ and
251 *C1qa*$^{\Delta M\varphi}$ mice.
252 **Figure supplement 4.** Flow cytometry gating strategy for comparison of innate lymphoid cell populations in *C1qa*$^{fl/fl}$
253 and *C1qa*$^{\Delta M\varphi}$ mice.
254
255
256

257 **C1q-expressing gut macrophages are located near enteric neurons**

258 Intestinal macrophages perform distinct functions depending on their anatomical location.
259 Macrophages in the lamina propria protect against invasion by pathogenic microbes and promote tissue
260 repair (Grainger et al., 2017). In contrast, macrophages that reside in deeper intestinal tissues, including the
261 submucosal plexus and muscularis (***Figure 4A***), regulate enteric smooth muscle cells and neurons that
262 drive gastrointestinal motility (De Schepper, Stakenborg, et al., 2018; De Schepper, Verheijden, et al.,
263 2018).

264 Immunofluorescence analysis revealed that C1q was located primarily beneath the lamina propria,
265 in a region consistent with the location of the submucosal plexus of the small intestine and colon (***Figure***
266 ***4A and B***). C1q was detected in a diffuse pattern close to macrophages in *C1qa*$^{fl/fl}$ mice and was absent in
267 *C1qa*$^{\Delta M\phi}$ mice (***Figure 4B***) despite the presence of similar overall numbers of CD169^{+} macrophages

268 (***Figure 4 – figure supplement 1***). Although we did not observe direct colocalization of C1q with CD169,
269 a macrophage marker that selectively marks nerve-adjacent macrophages (Ural et al., 2020), the pattern
270 was consistent with prior observations of C1q deposition in the extracellular matrix in the arterial wall (Cao
271 et al., 2003)(***Figure 4B***).

272 We next assessed the location of C1q relative to enteric neurons in the mouse small intestine.
273 Detection of the neuronal marker βIII tubulin (TUBB3) revealed the presence of two distinct layers of
274 enteric neurons: one just beneath the lamina propria that was consistent with the location of the submucosal
275 plexus, and one in the muscularis that was consistent with the location of the myenteric plexus (***Figure 4C***).
276 Immunofluorescence detection of C1q alongside TUBB3 revealed that C1q was located within an average
277 of ~5 μm of the nearest $TUBB3^+$ enteric neurons in the submucosal plexus and was largely absent from the
278 myenteric plexus (***Figure 4C***). Thus, C1q-producing gut macrophages are located close to enteric neurons
279 in the submucosal plexus.

280 C1q-producing intestinal macrophages exhibited several characteristics of nerve-adjacent
281 macrophages in other tissues. First, prior studies have shown that microglia in the central nervous system
282 and nerve-adjacent macrophages in peripheral tissues, such as the lung, are enriched for C1q gene
283 expression (Fonseca et al., 2017; Ural et al., 2020). This is consistent with our observations of C1q
284 expression in nerve-adjacent intestinal macrophages located in the submucosal plexus (***Figure 4C***). Second,
285 nerve-adjacent macrophages depend on a CSF1-CSF1R signaling axis for their maintenance and are
286 therefore sensitive to anti-CSF1R antibody-mediated depletion (Muller et al., 2014). Thus, our finding that
287 anti-CSF1R administration depleted C1q-expressing intestinal macrophages is consistent with their location
288 near enteric neurons (***Figure 2A-C***). Third, C1q-expressing intestinal macrophages showed elevated
289 expression of Arginase 1, CD169, and TREM2 (triggering receptor expressed on myeloid cells 2)(***Figure***
290 ***4D***), which are enriched on macrophages with known neuromodulatory functions (Colonna, 2003; Paloneva
291 et al., 2002; Ural et al., 2020). Thus, C1q-expressing intestinal macrophages are located near enteric neurons
292 and exhibit phenotypes characteristic of nerve-adjacent macrophages in other tissues.

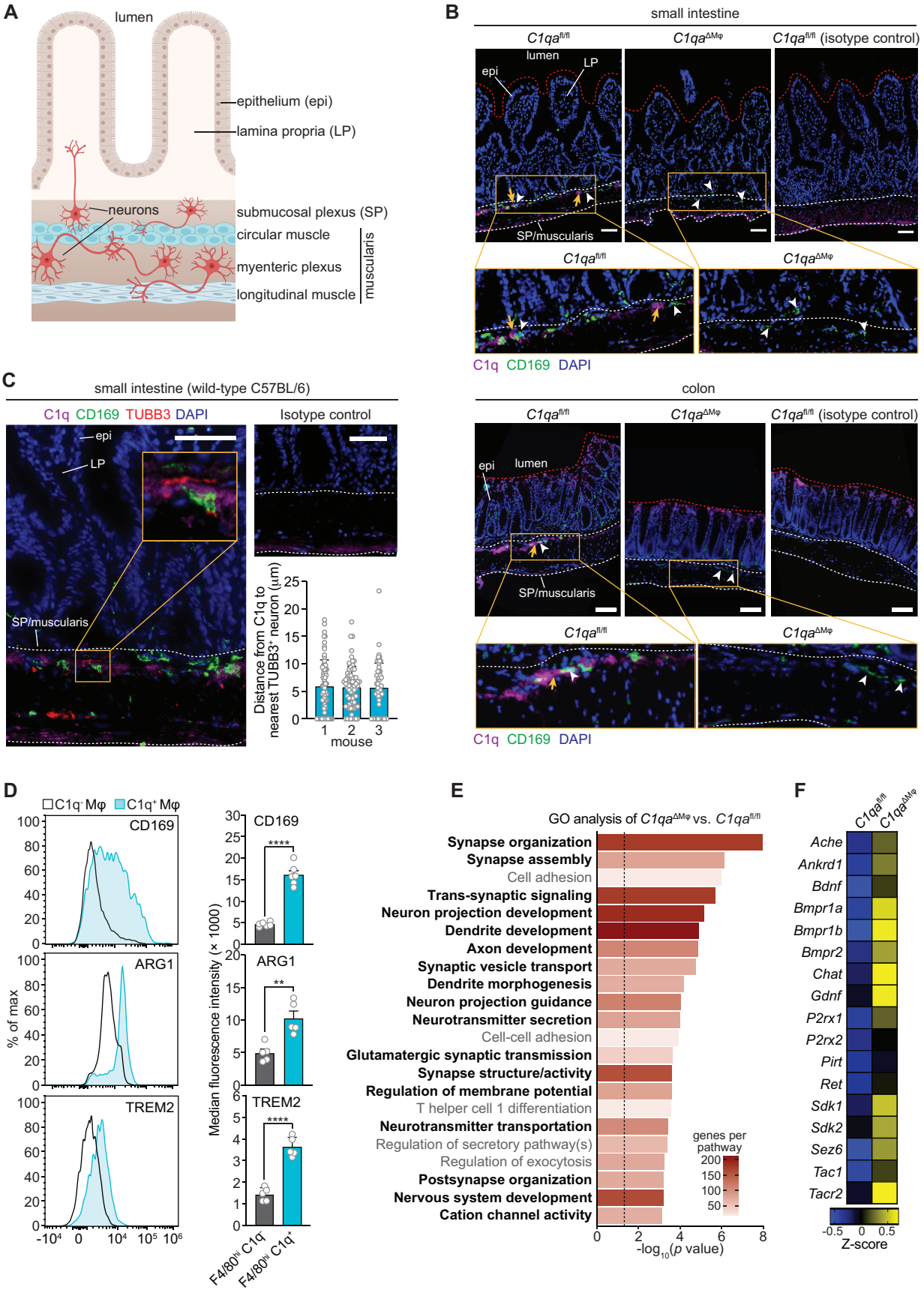
A
lumen
epithelium (epi)
lamina propria (LP)
neurons
submucosal plexus (SP)
circular muscle
myenteric plexus
longitudinal muscle
muscularis
B
small intestine
C1qa fl/fl
C1qa ΔMφ
C1qa fl/fl (isotype control)
epi
lumen
LP
SP/muscularis
C1q CD169 DAPI
C
small intestine (wild-type C57BL/6)
C1q CD169 TUBB3 DAPI
Isotype control
epi
LP
SP/muscularis
Distance from C1q to nearest TUBB3+ neuron (µm)
mouse
colon
D
C1q- Mφ
C1q+ Mφ
CD169
ARG1
TREM2
% of max
Median fluorescence intensity (× 1000)
F4/80hi C1q-
F4/80hi C1q+
E
GO analysis of C1qa ΔMφ vs. C1qa fl/fl
Synapse organization
Synapse assembly
Cell adhesion
Trans-synaptic signaling
Neuron projection development
Dendrite development
Axon development
Synaptic vesicle transport
Dendrite morphogenesis
Neuron projection guidance
Neurotransmitter secretion
Cell-cell adhesion
Glutamatergic synaptic transmission
Synapse structure/activity
Regulation of membrane potential
T helper cell 1 differentiation
Neurotransmitter transportation
Regulation of secretory pathway(s)
Regulation of exocytosis
Postsynapse organization
Nervous system development
Cation channel activity
genes per pathway
-log10(p value)
F
Ache
Ankrd1
Bdnf
Bmpr1a
Bmpr1b
Bmpr2
Chat
Gdnf
P2rx1
P2rx2
Pirt
Ret
Sdk1
Sdk2
Sez6
Tac1
Tacr2
Z-score

Figure 4. C1q-expressing macrophages are closely associated with neurons in the mouse intestine.
(A) Graphic depicting the muscularis of the mouse small intestine. The lumen, epithelium (epi), lamina propria (LP), submucosal plexus (SP), and distinct anatomical regions of the muscularis are indicated. Created at Biorender.com
(B) Immunofluorescence detection of C1q (violet) and macrophages marked with CD169 (green) in the small intestine and colon of *C1qa*$^{fl/fl}$ and *C1qa*$^{\Delta M\varphi}$ littermates. Nuclei were detected with 4',6-diamidino-2-phenylindole (DAPI; blue). Detection with isotype control antibodies on *C1qa*$^{fl/fl}$ small intestines is shown at right. Anti-rat IgG AlexaFluor 488 and streptavidin-Cy5 were used as secondary stains for CD169 and C1q respectively. The intestinal surface is denoted with a red dotted line and the gut lumen, epithelium, and lamina propria are indicated. The approximate region encompassing the submucosal plexus and the muscularis is denoted with two white dotted lines. Examples of C1q$^+$ areas are indicated with yellow arrows and examples of CD169$^+$ macrophages are indicated with white arrowheads. Note that the violet staining near the bottom of the muscularis is non-specific, as indicated by its presence in the isotype control image. Images are representative of three independent experiments. Scale bars = 50 μm.
(C) Immunofluorescence detection of C1q (violet), macrophages marked with CD169 (green) and neurons marked with TUBB3 (red) in the small intestines of wild-type C57BL/6 mice. Nuclei are detected with DAPI (blue). The epithelium, lamina propria are indicated. The approximate region encompassing the submucosal plexus and the muscularis is denoted with two white dotted lines. The expanded image area delineated by a yellow square shows an example of the close association between C1q and TUBB3$^+$ neurons. Images are representative of images captured from three mice. Anti-rat IgG AlexaFluor 488, anti-rabbit IgG AlexaFluor 594, and streptavidin-Cy5 were used as secondary stains for CD169, TUBB3, and C1q respectively, and an isotype control image is shown at upper right. Scale bars = 50 μm. Lower right panel: Distances between C1q$^+$ areas and the nearest TUBB3$^+$ neurons were measured in images captured from three mice. Each data point represents one measurement and measurements were made on 10 to 15 microscopic fields for each mouse (71, 70, and 57 total measurements, respectively).
(D) Flow cytometry analysis of CD169, Arginase 1, and TREM2 on C1q$^-$ and C1q$^+$ macrophages recovered from the small intestines of wild-type C57BL/6 mice. Median fluorescence intensities from multiple mice are quantified in the panels at right. Each data point represents one mouse (n=5-6 mice), and results are representative of two independent experiments. Error bars represent SEM. **$p<0.01$; ****$p<0.0001$ by two-tailed Student's t-test.
(E) Colonic longitudinal muscle myenteric plexus was acquired from *C1qa*$^{\Delta M\varphi}$ and *C1qa*$^{fl/fl}$ littermates. RNA-seq was performed, and annotated gene ontology (GO) biological processes were assigned to genes that were differentially expressed in *C1qa*$^{\Delta M\varphi}$ mice when compared to their *C1qa*$^{fl/fl}$ littermates. GO biological processes associated with neurons are in bold type. The dotted line indicates the cutoff for statistical significance. Five mice per group were analyzed as pooled biological replicates. Data are available from the Sequence Read Archive under BioProject ID PRJNA793870.
(F) Heat map of representative neuron-related genes differentially expressed in the colonic longitudinal muscle myenteric plexus of *C1qa*$^{\Delta M\varphi}$ mice relative to *C1qa*$^{fl/fl}$ littermates. Five mice per group were analyzed as pooled biological replicates.

Figure supplement 1. Similar numbers of CD169$^+$ macrophages are recovered from the small intestines of *C1qa*$^{\Delta M\varphi}$ and *C1qa*$^{fl/fl}$ littermates.

Figure supplement 2. The colonic muscle myenteric plexus of *C1qa*$^{\Delta M\varphi}$ mice has a transcriptional profile similar to that of mice with a gastrointestinal motility disorder.

C1qa$^{\Delta M\phi}$ mice have altered gastrointestinal motility

Macrophages engage in crosstalk with the enteric nervous system and regulate functions, including gastrointestinal motility, that depend on the enteric nervous system (Muller et al., 2014). This crosstalk involves the exchange of specific proteins such as bone morphogenetic protein 2 (BMP2) (Muller et al., 2014). Given that C1q$^+$ macrophages phenotypically resemble peripheral nerve-adjacent macrophages and

341 reside near enteric neurons, we postulated that macrophage-derived C1q might also regulate enteric nervous
342 system function.

343 As an initial test of this idea, we performed RNA-seq on the colonic longitudinal muscle-myenteric
344 plexus from *C1qa*$^{\Delta M\phi}$ and *C1qa*$^{fl/fl}$ littermates and then conducted unbiased Gene Set Enrichment Analysis.
345 Of the 22 biological pathways that were enriched in *C1qa*$^{\Delta M\phi}$ mice, 18 were related to neuronal development
346 or function, including synapse organization, dendrite development, and neurotransmitter secretion (***Figure***
347 ***4E and F***). 30 genes were differentially expressed when comparing the muscle-myenteric plexus of
348 *C1qa*$^{\Delta M\phi}$ and *C1qa*$^{fl/fl}$ mice. These included genes with known roles in regulating neuronal activity
349 (*Dusp26*), synaptic transmission (*Rasgrf2*), and neuropeptide signaling (*Tacr2*) (Mao et al., 2017;
350 Schwechter et al., 2013; Yang et al., 2017). We also compared the list of genes differentially expressed in
351 the *C1qa*$^{\Delta M\phi}$ mice to those differentially expressed in the *TashT* mouse line. This line contains an insertional
352 mutation that leads to a gut motility disorder comparable to Hirschsprung's disease, a human genetic
353 disorder resulting in incomplete development of the enteric nervous system (Bergeron et al., 2015). There
354 was a statistically significant overlap in the transcriptional changes in the colonic longitudinal muscle-
355 myenteric plexus of *C1qa*$^{\Delta M\phi}$ mice and *TashT* mice (***Figure 4 – figure supplement 2***). Together, these
356 results suggested that macrophage C1q impacts enteric nervous system gene expression and function.

357 Efficient coordination of gastrointestinal motility is necessary for proper digestion, nutrient
358 absorption, and excretion. Given that muscularis macrophages regulate enteric nervous system functions
359 that govern gastrointestinal motility (Muller et al., 2014), we assessed whether macrophage C1q impacts
360 gut motility. We first tested this idea by measuring gut transit time using the nonabsorbable dye carmine
361 red. *C1qa*$^{\Delta M\phi}$ and *C1qa*$^{fl/fl}$ littermates were gavaged with the dye and the time to first appearance of the dye
362 in the feces was recorded. Transit times were decreased in *C1qa*$^{\Delta M\phi}$ mice relative to their *C1qa*$^{fl/fl}$
363 littermates, indicating accelerated gut motility (***Figure 5A***). This was not due to a change in the lengths of
364 either the small intestine or the colon, which were unaltered in the *C1qa*$^{\Delta M\phi}$ mice (***Figure 5B***). By contrast,
365 gut transit time was unaltered in *C3*$^{-/-}$ mice, suggesting that macrophage C1q impacts gut motility

independent of its canonical function in the classical complement pathway (***Figure 5A***). Accelerated transit was also observed in the small intestines of *C1qa*$^{\Delta M\phi}$ mice as assessed by rhodamine dye transit assay (***Figure 5C***). We then conducted *ex vivo* colonic peristaltic recordings and observed that the colons of *C1qa*$^{\Delta M\phi}$ mice exhibited greater neuromuscular activity as compared to *C1qa*$^{fl/fl}$ littermates (***Figure 5 – figure supplement 1***). This suggested that the colons of *C1qa*$^{\Delta M\phi}$ mice maintained increased peristaltic activity compared to their *C1qa*$^{fl/fl}$ littermates even in the absence of gut-extrinsic signals. Finally, we directly assessed colonic motility by bead expulsion assay and found that *C1qa*$^{\Delta M\phi}$ mice had accelerated colonic transit *in vivo* (***Figure 5D***). Thus, the absence of macrophage C1q increases peristaltic activity and accelerates gut transit, indicating that macrophage C1q regulates gastrointestinal motility.

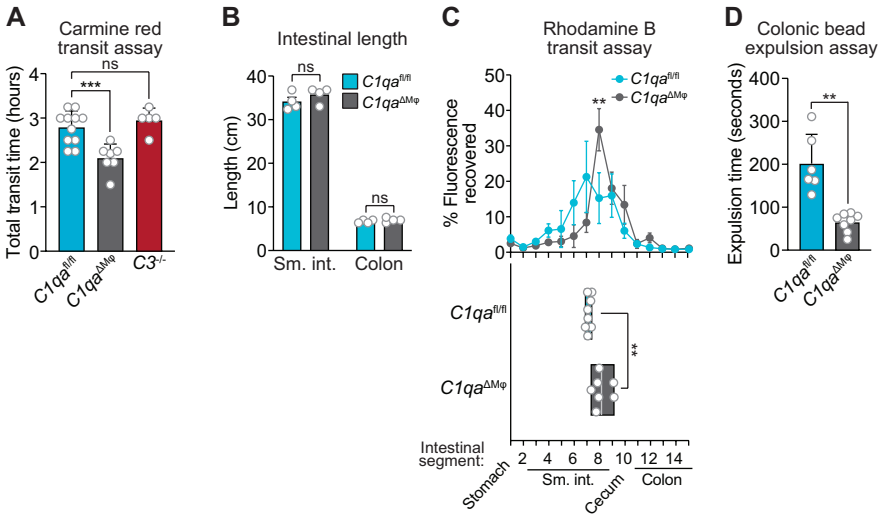

Figure 5. *C1qa*$^{\Delta M\varphi}$ mice have altered gastrointestinal motility.
(A) Measurement of total intestinal transit time in *C1qa*$^{fl/fl}$ and *C1qa*$^{\Delta M\varphi}$ littermates and *C3*$^{-/-}$ mice. Mice were gavaged with 100 µl of carmine red (5% (w/v in 1.5% methylcellulose). Fecal pellets were collected every 15 minutes and transit time was recorded when the dye was first observed in the feces. Each data point represents one mouse and the results are pooled from five independent experiments.
(B) Intestinal tract length is not altered in *C1qa*$^{\Delta M\varphi}$ mice. Small intestines and colons from *C1qa*$^{fl/fl}$ and *C1qa*$^{\Delta M\varphi}$ littermates were excised and measured. Each data point represents one mouse.
(C) Transit of rhodamine B-dextran through the intestines of *C1qa*$^{fl/fl}$ and *C1qa*$^{\Delta M\varphi}$ littermates. Mice were sacrificed 90 minutes after gavage with rhodamine B-dextran. The intestines were divided into 16 segments, the rhodamine B fluorescence was measured in each segment (top panel), and the geometric center of the fluorescence was determined for each mouse (bottom panel). Each data point represents one mouse and the results were pooled from four independent experiments.
(D) Colonic motility was measured by determining the expulsion time of a glass bead inserted intrarectally into *C1qa*$^{fl/fl}$ and *C1qa*$^{\Delta M\varphi}$ littermates. Each data point represents one mouse and the results are representative of three independent experiments.

392 sm. int., small intestine. Error bars represent SEM. **p<0.01; ***p<0.001; ns, not significant by two-tailed Student's
393 t-test.
394
395 **Figure supplements 1 and 2.** *Ex vivo* video recordings of colonic peristalsis in *C1qa*$^{fl/fl}$ and *C1qa*$^{\Delta M\varphi}$ littermates.
396

397

398 **DISCUSSION**

399 Here, we have identified a role for C1q in regulating gastrointestinal motility. We discovered that
400 nerve-adjacent macrophages are the primary source of C1q in the mouse intestine and that macrophage C1q
401 regulates enteric neuronal gene expression and gastrointestinal transit time. Our findings reveal a previously
402 unappreciated function for C1q in the intestine and help to illuminate the molecular basis for macrophage-
403 mediated control of gut motility.

404 Our study identifies macrophages as the main source of C1q in the mouse small intestine and colon.
405 Both transient antibody-mediated depletion of macrophages and *in vivo* deletion of the *C1qa* gene from
406 macrophages led to a marked reduction in intestinal *C1q* expression. The *C1qa*$^{\Delta M\phi}$ mice also lacked C1q in
407 the circulation, indicating that LysM^{+} macrophages or macrophage-like cells are also the source of
408 circulating C1q in the absence of infection. This enhances findings from prior studies indicating that
409 monocytes, macrophages, and immature dendritic cells are the main sources of C1q in the bloodstream (El-
410 Shamy et al., 2018). Importantly, the *C1qa*$^{\Delta M\phi}$ mice retained C1q expression in the brain, allowing us to
411 analyze the effects of C1q deficiency without possible confounding effects on the central nervous system.

412 C1q has two known physiological functions that are distinct and vary according to tissue context.
413 C1q was originally discovered as having a role in the classical complement pathway, which tags and
414 destroys invading microbes (Noris and Remuzzi, 2013; Schifferli et al., 1986). Circulating C1q binds to
415 invading microorganisms and recruits additional proteins that assemble into the membrane attack complex
416 (MAC) (Kishore and Reid, 2000). C1q-mediated MAC formation has been primarily described in the
417 bloodstream, where the necessary accessory proteins are present at high levels (Davis et al., 1979).
418 However, C1q is also expressed in the absence of infection in tissues such as the brain, where it regulates
419 neuronal development and function (Kouser et al., 2015; van Schaarenburg et al., 2016).

420 Our findings suggest that C1q does not play a central role in immune defense of the intestine. First,
421 we found that intestinal C1q expression was not induced by gut commensals or pathogens and was not
422 deposited into the gut lumen. Second, C1q deficiency did not markedly alter gut microbiota composition or
423 the course of disease after DSS treatment. There were also no major changes in cytokine expression or
424 numbers and frequencies of intestinal immune cells that would indicate dysregulated interactions with the
425 microbiota. Third, C1q was not required for clearance of *C. rodentium*, a non-disseminating enteric
426 pathogen whose clearance requires antigen-specific IgG and complement component 3 (C3) (Belzer et al.,
427 2011). Although we cannot rule out a role for C1q in immune defense against other intestinal pathogens,
428 these findings support the idea that C1q is not essential for intestinal immune defense in mice.

429 Instead, our results indicate that C1q influences enteric nervous system function and regulates
430 intestinal motility. First, most C1q-expressing macrophages were localized to the intestinal submucosal
431 plexus and were largely absent from the lamina propria. Second, C1q-expressing intestinal macrophages
432 were located close to submucosal plexus neurons and expressed cell surface markers like those expressed
433 by nerve-adjacent C1q-expressing macrophages in the lung (Ural et al., 2020). Third, macrophage-specific
434 deletion of *C1qa* altered enteric neuronal gene expression. Finally, consistent with the altered neuronal gene
435 expression, macrophage-specific *C1qa* deletion altered gastrointestinal motility in both the small and large
436 intestine. Thus, our results suggest that the function of C1q in the intestine is similar to its function in the
437 brain, where it regulates the development and function of neurons (Kouser et al., 2015; van Schaarenburg
438 et al., 2016).

439 A function for macrophage C1q in intestinal motility adds to the growing understanding of how gut
440 macrophages regulate intestinal peristalsis. Prior work has shown that CSF1R$^+$ macrophages selectively
441 localize to the muscularis of the mouse intestine (Muller et al., 2014; Gabanyi et al., 2016). These
442 macrophages secrete BMP2, which activates enteric neurons that regulate colonic muscle contraction and
443 thus colonic motility (Muller et al., 2014). We found that depletion of CSF1R$^+$ macrophages reduces
444 intestinal C1q expression, and that macrophage-specific deletion of *C1qa* alters enteric neuronal gene

445 expression and gut motility. Thus, our findings suggest that C1q is a key component of the macrophage-
446 enteric nervous system axis.

447 An important remaining question concerns the molecular mechanism by which C1q regulates gut
448 motility. One possibility is that C1q shapes microbiota composition which, in turn, impacts gut motility.
449 This idea is suggested by studies in zebrafish showing that a deficiency in intestinal macrophages leads to
450 altered gut microbiota composition relative to wild-type zebrafish (Earley et al., 2018). Other studies in
451 zebrafish and mice have shown that severe defects in enteric nervous system development produce changes
452 in gut microbiota composition that are linked to dysregulated gut motility (Rolig et al., 2017; Johnson et
453 al., 2018). However, we did not observe marked changes in the composition of the gut microbiota in
454 *C1qa*$^{\Delta M\phi}$ mice, arguing against a central role for the microbiota in C1q-mediated regulation of gut motility.
455 A second possibility is that the absence of C1q leads to immunological defects that alter gut transit time.
456 This idea is suggested by studies showing that T cell cytokines can influence gastrointestinal motility
457 (Akiho et al., 2011). However, this seems unlikely given the lack of pronounced immunological
458 abnormalities in the intestines of *C1qa*$^{\Delta M\phi}$ mice.

459 A third possibility is that C1q interacts directly with enteric neurons or glial cells. Like
460 macrophage-produced BMP2 (Muller et al., 2014), C1q might bind to specific receptors on neurons to
461 regulate their activity. In support of this idea, mouse enteric neurons express *Adgrb1*, which encodes BAI1
462 (Obata et al., 2020), a known C1q receptor on human neural stem cells (Benavente et al., 2020). Other
463 studies have suggested that C1q functions as a signaling effector on immune cells and neurons (Benoit &
464 Tenner, 2011; Ling et al., 2018). Macrophages have also been reported to restrain neurogenesis in the
465 enteric nervous system through phagocytosis of apoptotic neurons (Kulkarni et al., 2017). Given that C1q
466 can opsonize dying host cells (Botto et al., 1998; Korb and Ahearn, 1997), C1q could regulate enteric
467 nervous system function by tagging apoptotic neurons for elimination. It is also possible that C1q acts
468 directly on enteric smooth muscle cells that regulate gut motility. Although we cannot rule out this

469 possibility, our transcriptional profile of the colonic myenteric plexus of *C1qa*$^{\Delta M\phi}$ mice suggests that most
470 of the transcriptional changes were associated with neurons.

471 Our findings on intestinal C1q have implications for the understanding of human intestinal disease.
472 Dysregulated peristalsis is a characteristic of irritable bowel syndrome (Vrees et al., 2002) and is present in
473 a subset of inflammatory bowel disease patients (Bassotti et al., 2014). Our finding that macrophage C1q
474 regulates gut motility could suggest new strategies to prevent or treat these diseases. Additionally, most
475 humans with C1q deficiency develop systemic lupus erythematosus (SLE). Since C1q can target cellular
476 debris for phagocytosis, it is thought that the absence of C1q results in increased exposure of self-antigen
477 to the immune system, thereby reducing immune tolerance and causing autoimmune disease (Macedo and
478 Isaac, 2016). Furthermore, roughly 42.5% of SLE patients report gastrointestinal symptoms that range from
479 acute abdominal pain to chronic intestinal obstruction (Fawzy et al., 2016; Tian and Zhang, 2010). The
480 exact cause of these symptoms is unclear. Given that C1q deficiency is strongly correlated with SLE in
481 humans and alters gut motility in mice, we suggest that C1q could be a therapeutic target for SLE patients
482 that present with chronic constipation or other forms of dysregulated intestinal motility.

483

484

485 **MATERIALS AND METHODS**

486 **Key Resources Table**

Reagent type (species) or resource	Designation	Source or reference	Identifiers	Additional information
strain, strain background (*Mus musculus*)	*C1qa*$^{fl/fl}$; B6(SJL)-C1qa$^{tm1c(EUCOMM)Wtsi}$/TennJ	Jackson Laboratory; Fonseca et al., 2017	Stock #031261	
strain, strain background (*Mus musculus*)	LysM-Cre; B6.129P2-Lyz2$^{tm1(cre)Ifo}$/J	Jackson Laboratory; (Clausen et al., 1999)	Stock #004781	
strain, strain background (*Mus musculus*)	*C1qa*$^{\Delta M\phi}$	this paper		Generated by crossing *C1qa*$^{fl/fl}$ mice with LysM-Cre mice
strain, strain background (*Mus musculus*)	*C3*$^{-/-}$; B6.129S4-C3^{tm1Crr}/J	Jackson Laboratory; Wessels et al., 1995	Stock #029661	
strain, strain background (*Mus musculus*)	Germ-free C57BL/6J mice	UT Southwestern Gnotobiotics Core Facility		

Reagent type (species) or resource	Designation	Source or reference	Identifiers	Additional information
strain, strain background (*Salmonella enterica*)	*Salmonella enterica* subsp. enterica serovar Typhimurium strain SL1344	Dr. Vanessa Sperandio; Eichelberg and Galan, 1999		
strain, strain background (*Citrobacter rodentium*)	*Citrobacter rodentium* strain DBS100	ATCC	Strain# 51459	
antibody	Anti-Actin HRP (rabbit monoclonal)	Cell Signaling	Clone: 13E5	Immunoblot (1:5000)
antibody	Anti-ARG1 (sheep monoclonal)	R&D Systems	Clone: P05089	Flow (1:100)
antibody	Anti-B220 (rat monoclonal)	ThermoFisher	Clone: RA3-6B2	Flow (1:500)
antibody	Anti-C1q (rat monoclonal)	Cedarlane Laboratories	Clone: RmC7H8	Flow (1:50)
antibody	Anti-C1q (rabbit polyclonal)	ThermoFisher	Cat# PA5-29586	Immunoblot (1:500)
antibody	Anti-C1q-biotin (mouse monoclonal)	Abcam	Clone: JL1	ELISA (1:1000); Immunofluorescence (1:100)
antibody	Anti-CD3 (rat monoclonal)	ThermoFisher	Clone: 17A2	Flow (1:200)
antibody	Anti-CD4 (rat monoclonal)	BioLegend	Clone: GK1.5	Flow (1:500)
antibody	Anti-CD11b (rat monoclonal)	ThermoFisher	Clone: M1/70	Flow (1:200)
antibody	Anti-CD11c (Armenian hamster monoclonal)	ThermoFisher	Clone: N418	Flow (1:500)
antibody	Anti-CD16/32 (rat monoclonal)	BioLegend	Clone: 93	Fc receptor block (1:1000)
antibody	Anti-CD19 (rat monoclonal)	BioLegend	Clone: 1D3	Flow (1:500)
antibody	Anti-CD45 (rat monoclonal)	BioLegend	Clone: 30-F11	Flow (1:500)
antibody	Anti-CD90.2 (rat monoclonal)	BioLegend	Clone: 30-H12	Flow (1:500)
antibody	Anti-CD169 (rat monoclonal)	BioLegend	Clone: 3D6.112	Flow (1:200)
antibody	Anti-CD169 (rat monoclonal)	Abcam	Clone: 3D6.112	Immunofluorescence (1:200)
antibody	Anti-CSF1R (rat monoclonal)	Bio X Cell	Cat# AFS98	Macrophage depletion (dosage)
antibody	Anti-F4/80	BioLegend	Clone: BM8	Flow (1:100)
antibody	Anti-FoxP3 (rat monoclonal)	ThermoFisher	Clone: FJK-16s	Flow (1:50)
antibody	Anti-GATA3 (mouse monoclonal)	BD Biosciences	Clone: L50-823	Flow (1:50)
antibody	Anti-IgA (rat monoclonal)	ThermoFisher	Clone: 11-44-2	Flow (1:50)
antibody	Anti-LY6C	BioLegend	Clone: RB6-8C5	Flow (1:500)
antibody	Anti-MHCII	Thermo	Clone: M5/114.15.2	Flow (1:500)
antibody	Anti-REG3G antiserum (rabbit)	Cash et al., 2006; antiserum generated by Pacific Biosciences		Immunoblot (dilution)
antibody	Anti-RORγt	ThermoFisher	Clone: AFKJS-9	Flow (1:50)
antibody	Anti-T-BET	BioLegend	Clone: 4B10	Flow (1:50)
antibody	Anti-TREM2	R&D Systems	Clone: 237920	Flow (1:200)
antibody	Anti-TUBB3	Abcam	Cat# ab18207	Immunofluorescence (1:200)
antibody	Goat anti-rabbit IgG HRP conjugate	Abcam	Cat# ab6721	Immunoblot (1:5000)
antibody	secondary antibodies - AlexaFluor 488/594/647	Invitrogen		Immunofluorescence (1:400)
antibody	mouse IgG1	Abcam	Cat# ab18443	ELISA (10 μg/ml)
antibody	Rat IgG2a	ThermoFisher	Clone: 2A3	Isotype control for anti-CSF1R macrophage depletion
antibody	Rat IgG1 PE isotype control	Cedarlane Laboratories	Cat# CLCR104	Flow (1:50)
sequence-based reagent	mouse *C1qa* TaqMan assay	ThermoFisher	Assay ID: Mm00432142_m1	

Reagent type (species) or resource	Designation	Source or reference	Identifiers	Additional information
sequence-based reagent	mouse *C1qb* TaqMan assay	ThermoFisher	Assay ID: Mm01179619_m1	
sequence-based reagent	mouse *C1qc* TaqMan assay	ThermoFisher	Assay ID: Mm00776126_m1	
sequence-based reagent	mouse *Reg3g* TaqMan assay	ThermoFisher	Assay ID: Mm00441127_m1	
sequence-based reagent	mouse *Ifng* TaqMan assay	ThermoFisher	Assay ID: Mm01168134_m1	
sequence-based reagent	mouse *Il4* TaqMan assay	ThermoFisher	Assay ID: Mm00445259_m1	
sequence-based reagent	mouse *IL5* TaqMan assay	ThermoFisher	Assay ID: Mm00439646_m1	
sequence-based reagent	mouse *Il10* TaqMan assay	ThermoFisher	Assay ID: Mm01288386_m1	
sequence-based reagent	mouse *Il13* TaqMan assay	ThermoFisher	Assay ID: Mm00434204_m1	
sequence-based reagent	mouse *Il17a* TaqMan assay	ThermoFisher	Assay ID: Mm00439618_m1	
sequence-based reagent	mouse *Il17f* TaqMan assay	ThermoFisher	Assay ID: Mm00521423_m1	
sequence-based reagent	mouse 18*S* gene TaqMan assay	ThermoFisher	Assay ID: Mm03928990_g1	
sequence-based reagent	bacterial 16*S* V3 - rRNA gene forward primer	ThermoFisher; (Klindworth et al., 2013)	16*S* rRNA gene sequencing	5'-TCGTCGGCAGCGTCAGATGTGTATAAGAGACAGCCTACGGGNGGCWGCAG-3′
sequence-based reagent	bacterial 16*S* v4 - rRNA gene reverse primer	ThermoFisher; Klindworth et al., 2013	16*S* rRNA gene sequencing	5′-GTCTCGTGGGCTCGGAGATGTGTATAAGAGACAGGACTACHVGGGTATCTAATCC-3′
peptide, recombinant protein	recombinant mouse C1q	Complementech	Cat# M099	
commercial assay or kit	FOXP3/Transcription Factor Fixation/Permeabilization Buffer Set	ThermoFisher	Cat# 00-5523-00	
commercial assay or kit	MMLV Reverse Transcriptase Kit	ThermoFisher	Cat# 28025-021	
commercial assay or kit	PE300 (Paired end 300 bp) v3 kit	Illumina	Cat# MS-102-3001	
commercial assay or kit	RNeasy Universal Mini Kit	Qiagen	Cat# 73404	
commercial assay or kit	TaqMan Master Mix	ThermoFisher	Cat# 4369542	
commercial assay or kit	TruSeq RNA sample preparation kit	Illumina	Cat# RS-122-2001	
chemical compound, drug	Agencourt AmpureXP beads	Beckman Coulter Genomics	Cat# A63880	
chemical compound, drug	Carmine Red	Sigma	Cat# C1022-25G	
chemical compound, drug	Collagenase IV	Sigma	Cat# C5138-1G	
chemical compound, drug	Borosilicate glass beads (2mm)	Millipore Sigma	Cat# Z273627-1EA	
chemical compound, drug	Dextran sulfate sodium	Thomas Scientific	Cat# 216011090	
chemical compound, drug	DNase I	Sigma	Cat# DN25	
chemical compound, drug	Dispase II	Sigma	Cat# D4693-1G	
chemical compound, drug	FITC-dextran	Sigma	Cat# FD4-1g	
chemical compound, drug	Ghost 710	Tonbo Biosciences	Cat# 13-0871-T100	Flow cytometry viability dye
chemical compound, drug	Methylcellulose	Sigma	Cat# M0262-100G	
chemical compound, drug	Nalidixic acid, sodium salt	Research Products International	Cat# N23100-25.0	
chemical compound, drug	Optimal Cutting Temperature Compound (OCT)	ThermoFisher	Cat# 23-730-571	
chemical compound, drug	Percoll Plus	GE Healthcare	Cat# GE17-0891-09	

Reagent type (species) or resource	Designation	Source or reference	Identifiers	Additional information
chemical compound, drug	Protease inhibitors	Millipore Sigma	Cat# 11836153001	
chemical compound, drug	Rhodamine B-dextran	ThermoFisher	Cat# D1841	
chemical compound, drug	Streptavidin-Cy5	ThermoFisher	Cat# 434316	
chemical compound, drug	Streptavidin-HRP conjugate	Abcam	Cat# ab7403	ELISA
chemical compound, drug	VECTASHIELD Antifade Mounting Medium with DAPI	Vector Labs	Cat# H-1200-10	
software, algorithm	clusterProfiler			
software, algorithm	CLC Genomics Workbench			
software, algorithm	CLC Bio microbial genomics module			https:// digitalinsights.qiagen.com/plugins/clc-microbial-genomics-module/
software, algorithm	FlowJo			
software, algorithm	GraphPad PRISM	GraphPad Software	Version 7.0; RRID:SCR_002798	
software, algorithm	Igor Pro 9	WaveMetrics		
software, algorithm	Illumina Nextera Protocol	Illumina	Part # 15044223 Rev. B	
software, algorithm	ImageJ	National Institutes of Health		https://imagej.nih.gov/ij/
software, algorithm	NovoExpress	Agilent Technologies		
software, algorithm	PVCAM software	Teledyne Photometrics		
Other	Agilent 2100 Bioanalyzer	Agilent Technologies	G2939A	
Other	Amicon Ultra centrifugal filters	Millipore	Cat #UFC900324	
Other	BioRad ChemiDoc Touch System	BioRad	Cat# 1708370	
Other	CMOS camera	Teledyne Photometrics	MOMENT	
Other	Leica CM1950 (Cryostat)	Leica		
Other	FACSAria	BD Biosciences		
Other	Illumina MiSeq	Illumina	RRID:SCR_016379	
Other	Illumina NextSeq 500	Illumina		
Other	Keyence Fluorescence Microscope	Keyence	BZ-X800	
Other	NovoCyte 3005	Agilent Technologies		
Other	Organ bath chamber	Tokai Hit Co. (Japan)		
Other	Peristaltic pump	Gilson	MINIPULS3	
Other	QuantStudio 7 Flex Real-Time PCR System	Applied Biosystems	Cat #4485701	
Other	SpectraMax M5 plate reader	Molecular Devices		
Other	Zeiss Axio Imager M1 Microscope	Zeiss		

487

488

489 **Mice**

490 Wild-type C57BL/6J (Jackson Laboratory) and *C3*$^{-/-}$ mice (Jackson Laboratory; Wessels et al., 1995) were
491 bred and maintained in the SPF barrier facility at the University of Texas Southwestern Medical Center.
492 *C1qa*$^{\Delta M\phi}$ mice were generated by crossing *C1qa*$^{fl/fl}$ mice (Jackson Laboratory; Fonseca et al., 2017) with a
493 mouse expressing Cre recombinase controlled by the macrophage-specific mouse *Lyz2* promoter (LysM-

494 Cre mice; Jackson Laboratory; Clausen et al., 1999). Mice 8 to 12 weeks of age were used for all
495 experiments and cohoused littermates were used as controls. Both male and female mice were analyzed.
496 Germ-free C57BL/6J mice were bred and maintained in isolators at the University of Texas Southwestern
497 Medical Center. All procedures were performed in accordance with protocols approved by the Institutional
498 Animal Care and Use Committees (IACUC) of the UT Southwestern Medical Center.
499
500 **Quantitative polymerase chain reaction (qPCR)**
501 Tissue RNA was isolated using the RNeasy Universal Mini kit (Qiagen, Hilden, Germany). Cellular RNA
502 was isolated using the RNAqueous Micro kit (ThermoFisher). cDNA was generated from the purified RNA
503 using the M-MLV Reverse Transcriptase kit (ThermoFisher). qPCR analysis was performed using TaqMan
504 primer/probe sets and master mix (ThermoFisher) on a Quant-Studio 7 Flex Real-Time PCR System
505 (Applied Biosystems). Transcript abundances were normalized to 18*S* rRNA abundance. TaqMan probe
506 assay IDs are provided in the Key Resources table.
507
508 **Isolation and analysis of intestinal immune cells**
509 Lamina propria (LP) cells were isolated from the intestine using a published protocol (Yu et al., 2013; Yu
510 et al., 2014). Briefly, intestines were dissected from mice and Peyer's patches were removed. Intestines
511 were cut into small pieces and thoroughly washed with ice-cold phosphate-buffered saline (PBS) containing
512 5% fetal bovine serum (PBS-FBS). Epithelial cells were removed by incubating intestinal tissues in Hank's
513 buffered salt solution (HBSS) supplemented with 2 mM EDTA, followed by extensive washing with PBS-
514 FBS. Residual tissues were digested twice with Collagenase IV (Sigma), DNase I (Sigma) and Dispase (BD
515 Biosciences) for 45 minutes at 37°C with agitation. Cells were filtered through 70 μm cell strainers
516 (ThermoFisher) and applied onto a 40%:80% Percoll gradient (GE Healthcare). Subepithelial cell
517 populations were recovered at the interface of the 40% and 80% fractions. For small intestinal cell
518 suspensions, the epithelial fraction was kept and combined with enzymatically liberated subepithelial cells.
519 Cells were washed with 2 mM EDTA/3% FBS in PBS and Fc receptors were blocked with anti-CD16/32

520 (93). Cells were then stained with the viability dye Ghost 710 (Tonbo Biosciences) followed by antibodies
521 against cell surface markers including anti-CD45 (30-F11), anti-CD11b (M1/70), anti-MHCII
522 (M5/114.15.2), anti-F4/80 (BM8), anti-CD3 (17A2), anti-CD4 (GK1.5), anti-CD19 (1D3), anti-B220
523 (RA3-6B2), anti-CD11c (N418), anti-CD169 (3D6.112), anti-TREM2 (237920) and anti-LY6C (RB6-
524 8C5). Cells were fixed and permeabilized with the eBioscience FOXP3/Transcription Factor
525 Fixation/Permeabilization buffer set (ThermoFisher) and then subjected to intracellular staining with anti-
526 C1Q (RmC7H8), anti-FOXP3 (FJK-16s), anti-GATA3 (L50), anti-T-BET (4B10), anti-RORγ (AFKJS-9),
527 and anti-ARG1 (P05089). Cells were sorted using a FACSAria (BD Biosciences) or analyzed using a
528 NovoCyte 3005 (Agilent Technologies). Data were processed with FlowJo software (BD Biosciences) or
529 NovoExpress (Agilent Technologies).
530
531 **Macrophage depletion**
532 Anti-mouse CSF1R (ThermoFisher; AFS98) and rat IgG2a isotype control (ThermoFisher; 2A3) antibodies
533 were administered intraperitoneally at a concentration of 100 mg/kg. Mice were sacrificed 72 hours post-
534 injection and terminal ileum and colon were collected for qPCR analysis.
535
536 **Protein extraction from intestinal cells and feces**
537 To isolate proteins from intestinal cell suspensions, cell pellets were resuspended in 100 µl of RIPA Lysis
538 Buffer (ThermoFisher) supplemented with protease inhibitors (Millipore Sigma) and vortexed vigorously
539 every 5 minutes for 20 minutes. Lysates were cleared of cellular debris by centrifugation at 13000*g* for 5
540 minutes. To isolate proteins from the intestinal lumen, the entire gastrointestinal tract (from duodenum to
541 distal colon) was recovered from five wild-type C57BL/6J mice. The intestines were flushed with a total of
542 ~ 50 ml cold PBS containing protease inhibitors (Millipore Sigma, 11836153001). The flushes and fecal
543 pellets were homogenized by rotor and stator (TH Tissue Homogenizer; OMNI; TH01) and large particles
544 were centrifuged at 100*g* for 10 min at room temperature. The supernatants were carefully decanted and

545 centrifuged further at 3000*g* for 20 min at room temperature. The clarified supernatants were precipitated
546 with 40% ammonium sulfate overnight at 4°C. Precipitated protein was centrifuged at 3000*g* for 30 min at
547 4°C, then resuspended in cold 40% ammonium sulfate and centrifuged again. The pellets were resuspended
548 in room temperature PBS and allowed to mix for 10 min. Protein concentrations were determined by
549 Bradford assay (BioRad).
550
551 **Immunoblot**
552 50 μg of fecal protein or 25 μg of cellular protein was loaded onto a 4-20% gradient SDS-PAGE and
553 transferred to a PVDF membrane. Membranes were blocked in 5% nonfat dry milk in Tris-buffered saline
554 (TBS) with 0.1% Tween-20 and then incubated overnight with the following primary antibodies: anti-C1Q
555 (PA5-29586, ThermoFisher) and anti-actin (13E5, Cell Signaling). REG3G was detected by incubating
556 membranes with rabbit anti-REG3G antiserum (Cash et al., 2006). After washing, membranes were
557 incubated with goat anti-rabbit IgG HRP and then visualized with a BioRad ChemiDoc Touch system.
558
559 **Enzyme-linked immunosorbent assay (ELISA)**
560 Mouse C1q ELISA was performed as previously described (Petry et al., 2001). Briefly, microtiter plates
561 were coated overnight with mouse IgG1 and were then blocked with 5% BSA in PBS. Serum samples were
562 diluted 1:50 and plated for 1 hour at room temperature. After washing with 0.05% Tween-20 in PBS, bound
563 C1q was incubated with biotinylated anti-C1q antibody (JL1, Abcam). Biotinylated anti-C1q was detected
564 with a streptavidin-HRP conjugate (Abcam). Optical density was measured using a wavelength of 492 nm.
565 Plates were then analyzed using a SpectraMax M5 microplate reader (Molecular Devices).
566
567 **Intestinal permeability assay**
568 Intestinal permeability assays were performed by treating mice with fluorescein isothiocyanate dextran
569 (FITC-dextran) by oral gavage. The non-steroidal anti-inflammatory drug (NSAID) indomethacin was
570 administered to mice as a positive control. For the experimental group, mice were treated with 190 μl 7%

571 dimethyl sulfoxide (DMSO) in PBS by oral gavage. For the positive control group, mice were treated with
572 190 µl indomethacin (1.5 mg/ml in 7% DMSO in PBS) by oral gavage. After 1 hour, all mice were treated
573 with 190 ul FITC-dextran (80 mg/ml in PBS) by oral gavage. Mice were sacrificed after 4 hours and sera
574 were collected. Serum samples were centrifuged for 20 minutes at 4°C at 800*g* and supernatants were
575 collected. Serum FITC-dextran levels were measured by a fluorescence microplate assay against a standard
576 curve using a Spectramax plate reader (Molecular Devices).
577
578 **Dextran sulfate sodium (DSS) treatment**
579 Age and sex-matched mice were provided with 3% dextran sulfate sodium (weight/volume) in autoclaved
580 drinking water for 7 days. Animal weight and health were monitored in accordance with institutional
581 IACUC guidelines.
582
583 ***Salmonella* Typhimurium infection**
584 To prepare bacteria for infection, *Salmonella enterica* serovar Typhimurium (SL1344) was cultured in
585 Luria-Bertani (LB) broth containing 50 µg/ml streptomycin in a shaking incubator at 37ºC (Eichelberg and
586 Galan, 1999). The overnight culture was diluted the next day and grown to mid-log phase (OD_{600} = 0.3-
587 0.5). *C1qa*$^{fl/fl}$ and *C1qa*$^{\Delta M\phi}$ littermates were inoculated intragastrically with 10^9 CFU. All mice were
588 sacrificed 24 hours later and small intestinal tissues were harvested for analysis.
589
590 ***Citrobacter rodentium* infection**
591 To prepare bacteria for infection, an overnight culture of *C. rodentium* (DBS100, ATCC) in LB broth
592 containing nalidixic acid (100 µg/ml) in a shaking incubator at 37°C. The overnight culture was diluted the
593 next day and grown to mid-log phase (OD_{600} = 0.4-0.6). Bacteria were pelleted, washed, and resuspended
594 in PBS. Sex-matched littermates were inoculated intragastrically with 5×10^8 CFU. Fecal pellets were

595 collected at a fixed time every 48 hours, homogenized in sterile PBS, diluted, and plated on LB agar with
596 nalidixic acid (100 μg/ml).
597
598 **Immunofluorescence analysis of mouse intestines**
599 Mouse small intestines and colons were flushed with PBS and embedded with Optimal Cutting Temperature
600 compound (OCT) (ThermoFisher). Sections were fixed in ice cold acetone, blocked with 1% BSA, 10%
601 FBS, 1% Triton X-100 in PBS, and then incubated overnight at 4ºC with the following antibodies: mouse
602 anti-C1q biotin (JL-1), rat anti-CD169 (3D6.112), and rabbit anti-TUBB3 (ab18207, Abcam). Slides were
603 then washed with PBS containing 0.2% Tween-20 (PBS-T) and incubated with donkey anti-rabbit
604 AlexaFluor 488, donkey anti-rat AlexaFluor 594, and Streptavidin-Cy5 (ThermoFisher) for 1 hour at room
605 temperature in the dark. Slides were then washed in PBS-T and mounted with DAPI-Fluoromount-G
606 (Southern Biotech). Mounted slides were cured overnight at 4ºC until imaging.
607
608 **RNA-seq analysis of colonic longitudinal muscle myenteric plexus**
609 The colonic longitudinal muscle-myenteric plexus was collected from five age and sex matched *C1qa*$^{fl/fl}$
610 and *C1qa*$^{\Delta M\phi}$ mice by manual dissection using a 2 mm metal probe (Fisher Scientific). RNA was isolated
611 using the RNeasy Mini kit according to the manufacturer's protocol (Qiagen). Quantity and quality of RNA
612 samples was assessed on an Agilent 2100 Bioanalyzer (Agilent Technologies). RNA sequencing libraries
613 were prepared using the TruSeq RNA sample preparation kit (Illumina) according to the manufacturer's
614 protocol. Libraries were validated on an Agilent Bionalyzer 2100. Indexed libraries were sequenced on an
615 Illumina NextSeq550 for single-end 75 bp length reads. CLC Genomics Workbench 7 was used for
616 bioinformatics and statistical analysis of the sequencing data. The approach used by CLC Genomics
617 Workbench is based on a method developed previously (Mortazavi et al., 2008). To identify differentially
618 enriched biological pathways, all genes were ranked based on their $\log_2$ fold change and pathway
619 enrichment was identified using the R packages "clusterProfiler" and "msigdbr". For analysis of

620 differentially expressed genes, gene counts were analyzed using DESeq-2 and differentially expressed
621 genes were defined as having an adjusted p value <0.05. A Fisher's Exact Test was conducted to assess the
622 overlap between differentially expressed genes in *C1qa*$^{\Delta M\phi}$ mice and the TashT mouse (Bergeron et al.,
623 2015).
624
625 **16*S* rRNA gene sequencing and analysis**
626 The hypervariable regions V3 and V4 of the bacterial 16*S* rRNA gene were prepared using the Illumina
627 Nextera protocol (Part # 15044223 Rev. B). An amplicon of 460 bp was amplified using the 16*S* Forward
628 Primer and 16*S* Reverse Primer as described in the manufacturer's protocol. Primer sequences are given in
629 the Key Resources Table. The PCR product was purified using Agencourt AmpureXP beads (Beckman
630 Coulter Genomics). Illumina adapter and barcode sequences were ligated to the amplicon to attach them to
631 the MiSeqDx flow cell and for multiplexing. Quality and quantity of each sequencing library were assessed
632 using Bioanalyzer and picogreen measurements, respectively. Libraries were loaded onto a MiSeqDX flow
633 cell and sequenced using the Paired End 300 (PE300) v3 kit. Raw fastq files were demultiplexed based on
634 unique barcodes and assessed for quality. Samples with more than 50,000 quality control pass sequencing
635 reads were used for downstream analysis. Taxonomic classification and operational taxonomic unit analysis
636 were done using the CLC Microbial Genomics Module. Individual sample reads were annotated with the
637 Greengene database and taxonomic features were assessed.
638
639 **Gastrointestinal motility assays**
640 Motility assays were adapted from previous studies (Luo et al., 2018; Maurer, 2016; Muller et al., 2014).
641 To determine transit time through the entire gastrointestinal tract, mice were fasted overnight and water
642 was removed 1 hour prior to the start of the experiment. Mice were then singly housed for 1 hour and then
643 gavaged with 100 µl of carmine red (5% weight/volume; Sigma) in 1.5% methylcellulose. Fecal pellets
644 were collected every 15 minutes and transit time was recorded when the dye was first observed in the feces.

645 For small intestinal motility measurements, mice were fasted overnight and then gavaged with 100
646 μl of rhodamine B-dextran (5 mg/ml; ThermoFisher) in 2% methylcellulose. After 90 minutes, mice were
647 sacrificed and their stomachs, small intestines, ceca, and colons were collected. Small intestines were cut
648 into 8 segments of equal length and colons were cut into 5 segments of equal length. Segments were cut
649 open lengthwise and vortexed in 1 ml PBS to release rhodamine B-dextran. Fluorescence was then
650 measured on a SpectraMax M5 microplate reader (Molecular Devices). The geometric center of the dye
651 was calculated as: GC = Σ (% of total fluorescent signal per segment × segment number).
652 Relative fluorescence per segment was calculated as: (fluorescence signal in segment / total fluorescence
653 recovered) x 100.
654 To measure colonic motility, mice were fasted overnight and lightly anesthetized with isoflurane.
655 A 2 mm glass bead was inserted 2 cm intrarectally using a 2 mm surgical probe. Mice were then returned
656 to empty cages and time to reappearance of the bead was recorded.
657 To account for potential circadian differences in gut motility, the time of day for the initiation of
658 all experiments was held constant.
659
660 ***Ex vivo* peristaltic imaging**
661 *Ex vivo* video imaging and analysis of colonic peristalsis was carried out as described previously (Obata et
662 al., 2020). Colons were dissected, flushed with sterile PBS, and pinned into an organ bath chamber (Tokai
663 Hit, Japan) filled with high glucose Dulbecco's Modified Eagle Medium (DMEM). DMEM was oxygenated
664 (95% O2 and 5% CO_2), run through the chamber using a peristaltic pump (MINIPULS 3, Gilson) and kept
665 at 37°C. Colons were allowed to equilibrate to the organ chamber for 30 minutes before video recording.
666 Movies of colonic peristalsis were captured with a camera (MOMENT, Teledyne photometrics) using
667 PVCAM software (500ms time-lapse delay) over 15 minutes.
668
669

670 **Statistical analysis**

671 Graphed data are presented as means ± standard error of the mean (SEM). Statistics were determined with
672 GraphPad Prism software. Statistical analyses were performed using two-tailed Student's t test when
673 comparing two groups, one way ANOVA when comparing multiple groups, and Fisher's exact test to assess
674 overlap between groups of differentially expressed genes. The statistical tests used are indicated in the
675 figure legends. *$P \leq 0.05$; **$P \leq 0.01$; ***$P \leq 0.001$; and ns, $P > 0.05$.

676

677

678 **ADDITIONAL INFORMATION**

679 **Acknowledgements**

680 We thank Shai Bel for assistance with immunofluorescence imaging experiments, the UT Southwestern
681 Genomics Core for assistance with RNA sequencing experiments, and the UT Southwestern Flow
682 Cytometry Core for assistance with flow cytometry experiments. *Citrobacter rodentium* strain DBS100
683 was a gift from Vanessa Sperandio. This work was supported by NIH grants R01 DK070855 (L.V.H.),
684 Welch Foundation Grant I-1874 (L.V.H.), the Walter M. and Helen D. Bader Center for Research on
685 Arthritis and Autoimmune Diseases (L.V.H.), and the Howard Hughes Medical Institute (L.V.H.). M.P.
686 and A.A.C. were supported by NIH T32 AI005284. E.K. was supported by NIH F31 DK126391. Y.O. is
687 the Nancy Cain Marcus and Jeffrey A. Marcus Scholar in Medical Research, in Honor of Dr. Bill S. Vowell.

688

689 **Competing interests:** The authors declare no competing interests.

690

691 **Author contributions**

692 Mihir Pendse, Conceptualization, Investigation, Data curation, Formal analysis, Methodology, Supervision,
693 Writing – original draft, Writing – review and editing; Yun Li, Investigation; Cristine N. Salinas,
694 Investigation; Gabriella Quinn, Data curation, Formal analysis; Daniel C. Propheter, Investigation, Writing
695 – review and editing; Chaitanya Dende, Investigation, Writing – review and editing; Alexander A. Crofts,

Data curation, Formal analysis; Eugene Koo, Methodology; Brian Hassell, Investigation; Kelly A. Ruhn, Investigation; Prithvi Raj, Investigation, Data curation, Formal analysis; Yuuki Obata, Investigation, Methodology, Writing – original draft, Writing – review and editing; Lora V. Hooper, Conceptualization, Funding acquisition, Supervision, Writing – original draft, Writing – review and editing.

Data availability

16*S* rRNA gene sequencing data (***Figure 3D***) and RNA sequencing data (***Figure 4E and F; Figure 4 – figure supplement 2***) are available from the Sequence Read Archive under BioProject ID PRJNA793870. All mouse strains used are available commercially.

REFERENCES

Akiho, H., Ihara, E., Motomura, Y., Nakamura, K. (2011). Cytokine-induced alterations of gastrointestinal motility in gastrointestinal disorders. *World J Gastrointest Pathophysiol, 2*, 72-81. https://doi.org/10.4291/wjgp.v2.i5.72

Bassotti, G., Antonelli, E., Villanacci, V., Salemme, M., Coppola, M., Annese, V. (2014). Gastrointestinal motility disorders in inflammatory bowel diseases. *World J Gastroenterol, 20*, 37-44. https://doi.org/10.3748/wjg.v20.i1.37

Belzer, C., Liu, Q., Carroll, M. C., Bry, L. (2011). The role of specific IgG and complement in combating a primary mucosal infection of the gut epithelium. *Eur J Microbiol Immunol (Bp), 1*, 311-318. https://doi.org/10.1556/EuJMI.1.2011.4.7

Benavente, F., Piltti, K.M., Hooshmand, M.J., Nava, A.A., Lakatos, A., Feld, B.G., Creasman, D., Gershon, P.D., Anderson, A. (2020). Novel C1q receptor-mediated signaling controls neural stem cell behavior and neurorepair. *eLife, 9*, e55732. https://doi.org/10.7554/eLife.55732

Benoit, M. E., Tenner, A. J. (2011). Complement protein C1q-mediated neuroprotection is correlated with regulation of neuronal gene and microRNA expression. *J Neurosci, 31*, 3459-3469. https://doi.org/10.1523/JNEUROSCI.3932-10.2011

Bergeron, K. F., Cardinal, T., Toure, A. M., Beland, M., Raiwet, D. L., Silversides, D. W., Pilon, N. (2015). Male-biased aganglionic megacolon in the TashT mouse line due to perturbation of silencer elements in a large gene desert of chromosome 10. *PLoS Genet, 11*, e1005093. https://doi.org/10.1371/journal.pgen.1005093

736 Bogunovic, M., Ginhoux, F., Helft, J., Shang, L., Hashimoto, D., Greter, M., Liu, K., Jakubzick, C.,
737 Ingersoll, M. A., Leboeuf, M., Stanley, E. R., Nussenzweig, M., Lira, S. A., Randolph, G. J., Merad, M.
738 (2009). Origin of the lamina propria dendritic cell network. *Immunity, 31*, 513-525.
739 https://doi.org/10.1016/j.immuni.2009.08.010
740
741 Bossi, F., Tripodo, C., Rizzi, L., Bulla, R., Agostinis, C., Guarnotta, C., Munaut, C., Baldassarre, G., Papa,
742 G., Zorzet, S., Ghebrehiwet, B., Ling, G. S., Botto, M., Tedesco, F. (2014). C1q as a unique player in
743 angiogenesis with therapeutic implication in wound healing. *Proc Natl Acad Sci U S A, 111*, 4209-4214.
744 https://doi.org/10.1073/pnas.1311968111
745
746 Botto, M., Dell'Agnola, C., Bygrave, A. E., Thompson, E. M., Cook, H. T., Petry, F., Loos, M., Pandolfi,
747 P. P., Walport, M. J. (1998). Homozygous C1q deficiency causes glomerulonephritis associated with
748 multiple apoptotic bodies. *Nat Genet, 19*, 56-59. https://doi.org/10.1038/ng0598-56
749
750 Cao, W., Bobryshev, Y. V., Lord, R. S., Oakley, R. E., Lee, S. H., Lu, J. (2003). Dendritic cells in the
751 arterial wall express C1q: potential significance in atherogenesis. *Cardiovasc Res, 60*, 175-186.
752 https://doi.org/10.1016/s0008-6363(03)00345-6
753
754 Casals, C., Garcia-Fojeda, B., Minutti, C. M. (2019). Soluble defense collagens: Sweeping up immune
755 threats. *Mol Immunol, 112*, 291-304. https://doi.org/10.1016/j.molimm.2019.06.007
756
757 Cash, H. L., Whitham, C. V., Behrendt, C. L., Hooper, L. V. (2006). Symbiotic bacteria direct expression
758 of an intestinal bactericidal lectin. *Science, 313*, 1126-1130. https://doi.org/10.1126/science.1127119
759
760 Chu, Y., Jin, X., Parada, I., Pesic, A., Stevens, B., Barres, B., Prince, D. A. (2010). Enhanced synaptic
761 connectivity and epilepsy in C1q knockout mice. *Proc Natl Acad Sci U S A, 107*, 7975-7980.
762 https://doi.org/10.1073/pnas.0913449107
763
764 Clausen, B. E., Burkhardt, C., Reith, W., Renkawitz, R., Forster, I. (1999). Conditional gene targeting in
765 macrophages and granulocytes using LysMcre mice. *Transgenic Res, 8*, 265-277.
766 https://doi.org/10.1023/a:1008942828960
767
768 Colonna, M. (2003). TREMs in the immune system and beyond. *Nat Rev Immunol, 3*, 445-453.
769 https://doi.org/10.1038/nri1106
770
771 Davis, C. A., Vallota, E. H., Forristal, J. (1979). Serum complement levels in infancy: age related changes.
772 *Pediatr Res, 13*, 1043-1046. https://doi.org/10.1203/00006450-197909000-00019
773
774 De Schepper, S., Stakenborg, N., Matteoli, G., Verheijden, S., Boeckxstaens, G. E. (2018). Muscularis
775 macrophages: Key players in intestinal homeostasis and disease. *Cell Immunol, 330*, 142-150.
776 https://doi.org/10.1016/j.cellimm.2017.12.009
777
778 De Schepper, S., Verheijden, S., Aguilera-Lizarraga, J., Viola, M. F., Boesmans, W., Stakenborg, N.,
779 Voytyuk, I., Schmidt, I., Boeckx, B., Dierckx de Casterle, I., Baekelandt, V., Gonzalez Dominguez, E.,
780 Mack, M., Depoortere, I., De Strooper, B., Sprangers, B., Himmelreich, U., Soenen, S., Guilliams, M.,
781 Vanden Berghe, P., Jones, E., Lambrechts, D., Boeckxstaens, G. (2018, Oct 4). Self-maintaining gut
782 macrophages are essential for intestinal homeostasis. *Cell, 175*, 400-415 e413.
783 https://doi.org/10.1016/j.cell.2018.07.048
784

785 Earley, A.M., Graves, C.L., Shiau, C.E. (2018). Critical role for a subset of intestinal macrophages in
786 shaping gut microbiota in adult zebrafish. *Cell Rep, 25*, 424-436. https://doi.org/
787 10.1016/j.celrep.2018.09.025
788
789 Eichelberg, K., Galan, J. E. (1999). Differential regulation of Salmonella typhimurium type III secreted
790 proteins by pathogenicity island 1 (SPI-1)-encoded transcriptional activators InvF and hilA. *Infect Immun,*
791 *67*, 4099-4105. https://doi.org/10.1128/IAI.67.8.4099-4105.1999
792
793 El-Shamy, A., Branch, A. D., Schiano, T. D., & Gorevic, P. D. (2018). The complement system and C1q
794 in chronic hepatitis C virus infection and mixed cryoglobulinemia. *Front Immunol, 9*, 1001.
795 https://doi.org/10.3389/fimmu.2018.01001
796
797 Fawzy, M., Edrees, A., Okasha, H., El Ashmaui, A., Ragab, G. (2016). Gastrointestinal manifestations in
798 systemic lupus erythematosus. *Lupus, 25*, 1456-1462. https://doi.org/10.1177/0961203316642308
799
800 Fonseca, M. I., Chu, S. H., Hernandez, M. X., Fang, M. J., Modarresi, L., Selvan, P., MacGregor, G. R.,
801 Tenner, A. J. (2017). Cell-specific deletion of C1qa identifies microglia as the dominant source of C1q in
802 mouse brain. *J Neuroinflammation, 14*, 48. https://doi.org/10.1186/s12974-017-0814-9
803
804 Gabanyi, I., Muller, P. A., Feighery, L., Oliveira, T. Y., Costa-Pinto, F. A., Mucida, D. (2016). Neuro-
805 immune interactions drive tissue programming in intestinal macrophages. *Cell, 164*, 378-391.
806 https://doi.org/10.1016/j.cell.2015.12.023
807
808 Gattu, S., Bang, Y. J., Pendse, M., Dende, C., Chara, A. L., Harris, T. A., Wang, Y., Ruhn, K. A., Kuang,
809 Z., Sockanathan, S., Hooper, L. V. (2019). Epithelial retinoic acid receptor beta regulates serum amyloid A
810 expression and vitamin A-dependent intestinal immunity. *Proc Natl Acad Sci U S A, 116*, 10911-10916.
811 https://doi.org/10.1073/pnas.1812069116
812
813 Grainger, J. R., Konkel, J. E., Zangerle-Murray, T., Shaw, T. N. (2017). Macrophages in gastrointestinal
814 homeostasis and inflammation. *Pflugers Arch, 469*, 527-539. https://doi.org/10.1007/s00424-017-1958-2
815
816 Hammond, J. W., Bellizzi, M. J., Ware, C., Qiu, W. Q., Saminathan, P., Li, H., Luo, S., Ma, S. A., Li, Y.,
817 Gelbard, H. A. (2020). Complement-dependent synapse loss and microgliosis in a mouse model of multiple
818 sclerosis. *Brain Behav Immun, 87*, 739-750. https://doi.org/10.1016/j.bbi.2020.03.004
819
820 Hong, S., Beja-Glasser, V. F., Nfonoyim, B. M., Frouin, A., Li, S., Ramakrishnan, S., Merry, K. M., Shi,
821 Q., Rosenthal, A., Barres, B. A., Lemere, C. A., Selkoe, D. J., Stevens, B. (2016). Complement and
822 microglia mediate early synapse loss in Alzheimer mouse models. *Science, 352*, 712-716.
823 https://doi.org/10.1126/science.aad8373
824
825 Johnson, C.D., Barlow-Anacker, A.J., Pierre, J.F., Touw, K., Erickson, C.S., Furness, J.B., Epstein, M.L.,
826 Gosain, A. (2018). Deletion of choline acetyltransferase in enteric neurons results in postnatal intestinal
827 dysmotility and dysbiosis. *FASEB J, 32*, 4744–4752. https://doi.org/10.1096/fj.201701474RR
828
829 Kishore, U., Reid, K. B. (2000). C1q: structure, function, and receptors. *Immunopharmacology, 49*, 159-
830 170. https://doi.org/10.1016/s0162-3109(00)80301-x
831

832 Klindworth, A., Pruesse, E., Schweer, T., Peplies, J., Quast, C., Horn, M., Glockner, F. O. (2013).
833 Evaluation of general 16S ribosomal RNA gene PCR primers for classical and next-generation sequencing-
834 based diversity studies. *Nucleic Acids Res, 41*, e1. https://doi.org/10.1093/nar/gks808
835
836 Korb, L. C., Ahearn, J. M. (1997). C1q binds directly and specifically to surface blebs of apoptotic human
837 keratinocytes: complement deficiency and systemic lupus erythematosus revisited. *J Immunol, 158*, 4525-
838 4528. https://www.ncbi.nlm.nih.gov/pubmed/9144462
839
840 Kouser, L., Madhukaran, S. P., Shastri, A., Saraon, A., Ferluga, J., Al-Mozaini, M., Kishore, U. (2015).
841 Emerging and novel functions of complement protein C1q. *Front Immunol, 6*, 317.
842 https://doi.org/10.3389/fimmu.2015.00317
843
844 Kulkarni, S., Micci, M. A., Leser, J., Shin, C., Tang, S. C., Fu, Y. Y., Liu, L., Li, Q., Saha, M., Li, C.,
845 Enikolopov, G., Becker, L., Rakhilin, N., Anderson, M., Shen, X., Dong, X., Butte, M. J., Song, H.,
846 Southard-Smith, E. M., Kapur, R. P., Bogunovic, M., Pasricha, P. J. (2017). Adult enteric nervous system
847 in health is maintained by a dynamic balance between neuronal apoptosis and neurogenesis. *Proc Natl Acad*
848 *Sci USA, 114*, E3709-E3718. https://doi.org/10.1073/pnas.1619406114
849
850 Ling, G. S., Crawford, G., Buang, N., Bartok, I., Tian, K., Thielens, N. M., Bally, I., Harker, J. A., Ashton-
851 Rickardt, P. G., Rutschmann, S., Strid, J., Botto, M. (2018). C1q restrains autoimmunity and viral infection
852 by regulating CD8+ T cell metabolism. *Science, 360*, 558-563. https://doi.org/10.1126/science.aao4555
853
854 Luo, J., Qian, A., Oetjen, L. K., Yu, W., Yang, P., Feng, J., Xie, Z., Liu, S., Yin, S., Dryn, D., Cheng, J.,
855 Riehl, T. E., Zholos, A. V., Stenson, W. F., Kim, B. S., Hu, H. (2018,). TRPV4 channel signaling in
856 macrophages promotes gastrointestinal motility via direct effects on smooth muscle cells. *Immunity, 49*,
857 107-119 e104. https://doi.org/10.1016/j.immuni.2018.04.021
858
859 Macedo, A. C., Isaac, L. (2016). Systemic lupus erythematosus and deficiencies of early components of the
860 complement classical pathway. *Front Immunol, 7*, 55. https://doi.org/10.3389/fimmu.2016.00055
861
862 Mao, Y. L., Shen, C. L., Zhou, T., Ma, B. T., Tang, L. Y., Wu, W. T., Zhang, H. X., Lu, H. L., Xu, W. X.,
863 Wang, Z. G. (2017). Ablation of Tacr2 in mice leads to gastric emptying disturbance. *Neurogastroenterol*
864 *Motil, 29*, e13117. https://doi.org/10.1111/nmo.13117
865
866 Matheis, F., Muller, P. A., Graves, C. L., Gabanyi, I., Kerner, Z. J., Costa-Borges, D., Ahrends, T.,
867 Rosenstiel, P., Mucida, D. (2020). Adrenergic signaling in muscularis macrophages limits infection-
868 induced neuronal loss. *Cell, 180*, 64-78 e16. https://doi.org/10.1016/j.cell.2019.12.002
869
870 Maurer, A. H. (2016). Gastrointestinal motility, part 2: small-bowel and colon transit. *J Nucl Med Technol,*
871 *44*, 12-18. https://doi.org/10.2967/jnumed.113.134551
872
873 Mortazavi, A., Williams, B. A., McCue, K., Schaeffer, L., Wold, B. (2008). Mapping and quantifying
874 mammalian transcriptomes by RNA-Seq. *Nat Methods, 5*, 621-628. https://doi.org/10.1038/nmeth.1226
875
876 Muller, P. A., Koscso, B., Rajani, G. M., Stevanovic, K., Berres, M. L., Hashimoto, D., Mortha, A.,
877 Leboeuf, M., Li, X. M., Mucida, D., Stanley, E. R., Dahan, S., Margolis, K. G., Gershon, M. D., Merad,
878 M., Bogunovic, M. (2014). Crosstalk between muscularis macrophages and enteric neurons regulates
879 gastrointestinal motility. *Cell, 158*, 300-313. https://doi.org/10.1016/j.cell.2014.04.050
880

881 Noris, M., Remuzzi, G. (2013). Overview of complement activation and regulation. *Semin Nephrol, 33*,
882 479-492. https://doi.org/10.1016/j.semnephrol.2013.08.001
883
884 Obata, Y., Castaño, A., Boeing, S., Bon-Frauches, A.C., Fung, C., Fallesen, T., de Agüero, M.G., Yilmaz,
885 B., Lopes, R., Huseynova, A., Horswell, S., Maradana, M.R., Boesmans, W., Vanden Berghe, P., Murray,
886 A.J., Stockinger, B., Macpherson, A.J., Pachnis, V. (2020). Neuronal programming by microbiota regulates
887 intestinal physiology. *Nature, 578*, 284-289. https://doi.org/10.1038/s41586-020-1975-8
888
889 Paloneva, J., Manninen, T., Christman, G., Hovanes, K., Mandelin, J., Adolfsson, R., Bianchin, M., Bird,
890 T., Miranda, R., Salmaggi, A., Tranebjaerg, L., Konttinen, Y., Peltonen, L. (2002). Mutations in two genes
891 encoding different subunits of a receptor signaling complex result in an identical disease phenotype. *Am J*
892 *Hum Genet, 71*, 656-662. https://doi.org/10.1086/342259
893
894 Petry, F., Botto, M., Holtappels, R., Walport, M. J., Loos, M. (2001). Reconstitution of the complement
895 function in C1q-deficient (C1qa-/-) mice with wild-type bone marrow cells. *J Immunol, 167*, 4033-4037.
896 https://doi.org/10.4049/jimmunol.167.7.4033
897
898 Rao, M., Gershon, M. D. (2016). The bowel and beyond: the enteric nervous system in neurological
899 disorders. *Nat Rev Gastroenterol Hepatol, 13*, 517-528. https://doi.org/10.1038/nrgastro.2016.107
900
901 Rolig, A.S., Mittge, E.K., Ganz, J., Troll, J.V., Melancon, E., Wiles, T.J., Alligood, K., Stephens, W.Z.,
902 Eisen, J.S., Guillemin, K. (2017). The enteric nervous system promotes intestinal health by constraining
903 microbiota composition. *PLoS Biol*, 15, e2000689. https://doi.org/10.1371/journal.pbio.2000689
904
905 Schifferli, J. A., Ng, Y. C., Peters, D. K. (1986). The role of complement and its receptor in the elimination
906 of immune complexes. *N Engl J Med, 315*, 488-495. https://doi.org/10.1056/NEJM198608213150805
907
908 Schwechter, B., Rosenmund, C., Tolias, K. F. (2013). RasGRF2 Rac-GEF activity couples NMDA receptor
909 calcium flux to enhanced synaptic transmission. *Proc Natl Acad Sci USA, 110*, 14462-14467.
910 https://doi.org/10.1073/pnas.1304340110
911
912 Shah, D., Romero, F., Zhu, Y., Duong, M., Sun, J., Walsh, K., Summer, R. (2015). C1q deficiency promotes
913 pulmonary vascular inflammation and enhances the susceptibility of the lung endothelium to injury. *J Biol*
914 *Chem, 290*, 29642-29651. https://doi.org/10.1074/jbc.M115.690784
915
916 Thielens, N. M., Tedesco, F., Bohlson, S. S., Gaboriaud, C., Tenner, A. J. (2017). C1q: A fresh look upon
917 an old molecule. *Mol Immunol, 89*, 73-83. https://doi.org/10.1016/j.molimm.2017.05.025
918
919 Tian, X. P., Zhang, X. (2010). Gastrointestinal involvement in systemic lupus erythematosus: insight into
920 pathogenesis, diagnosis and treatment. *World J Gastroenterol, 16*, 2971-2977.
921 https://doi.org/10.3748/wjg.v16.i24.2971
922
923 Ural, B. B., Yeung, S. T., Damani-Yokota, P., Devlin, J. C., de Vries, M., Vera-Licona, P., Samji, T., Sawai,
924 C. M., Jang, G., Perez, O. A., Pham, Q., Maher, L., Loke, P., Dittmann, M., Reizis, B., Khanna, K. M.
925 (2020). Identification of a nerve-associated, lung-resident interstitial macrophage subset with distinct
926 localization and immunoregulatory properties. *Sci Immunol, 5*.
927 https://doi.org/10.1126/sciimmunol.aax8756
928

929 van Schaarenburg, R. A., Suurmond, J., Habets, K. L., Brouwer, M. C., Wouters, D., Kurreeman, F. A.,
930 Huizinga, T. W., Toes, R. E., Trouw, L. A. (2016). The production and secretion of complement component
931 C1q by human mast cells. *Mol Immunol, 78*, 164-170. https://doi.org/10.1016/j.molimm.2016.09.001
932
933 Vrees, M. D., Pricolo, V. E., Potenti, F. M., Cao, W. (2002). Abnormal motility in patients with ulcerative
934 colitis: the role of inflammatory cytokines. *Arch Surg, 137*, 439-445.
935 https://doi.org/10.1001/archsurg.137.4.439
936
937 Warren, J., Mastroeni, P., Dougan, G., Noursadeghi, M., Cohen, J., Walport, M. J., Botto, M. (2002).
938 Increased susceptibility of C1q-deficient mice to Salmonella enterica serovar Typhimurium infection. *Infect*
939 *Immun, 70*, 551-557. https://doi.org/10.1128/IAI.70.2.551-557.2002
940
941 Wessels, M. R., Butko, P., Ma, M., Warren, H. B., Lage, A. L., Carroll, M. C. (1995). Studies of group B
942 streptococcal infection in mice deficient in complement component C3 or C4 demonstrate an essential role
943 for complement in both innate and acquired immunity. *Proc Natl Acad Sci U S A, 92*, 11490-11494.
944 https://doi.org/10.1073/pnas.92.25.11490
945
946 Yang, C. H., Yeh, Y. J., Wang, J. Y., Liu, Y. W., Chen, Y. L., Cheng, H. W., Cheng, C. M., Chuang, Y. J.,
947 Yuh, C. H., Chen, Y. R. (2017). NEAP/DUSP26 suppresses receptor tyrosine kinases and regulates
948 neuronal development in zebrafish. *Sci Rep, 7*, 5241. https://doi.org/10.1038/s41598-017-05584-7
949
950 Yu, X., Rollins, D., Ruhn, K. A., Stubblefield, J. J., Green, C. B., Kashiwada, M., Rothman, P. B.,
951 Takahashi, J. S., Hooper, L. V. (2013). TH17 cell differentiation is regulated by the circadian clock. *Science,*
952 *342*, 727-730. https://doi.org/10.1126/science.1243884
953
954 Yu, X., Wang, Y., Deng, M., Li, Y., Ruhn, K. A., Zhang, C. C., Hooper, L. V. (2014). The basic leucine
955 zipper transcription factor NFIL3 directs the development of a common innate lymphoid cell precursor.
956 *Elife, 3, e04406*. https://doi.org/10.7554/eLife.04406
957
958
959
960

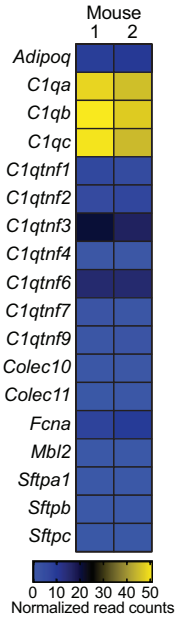

Figure 1 - figure supplement 1. C1q is expressed in the mouse colon.
RNA-seq analysis of soluble defense collagen expression in the colons of C57BL/6 mice. Data were reanalyzed from Gattu et al., 2019. Each column represents one mouse. Data are available in the Gene Expression Omnibus repository under accession number GSE122471.

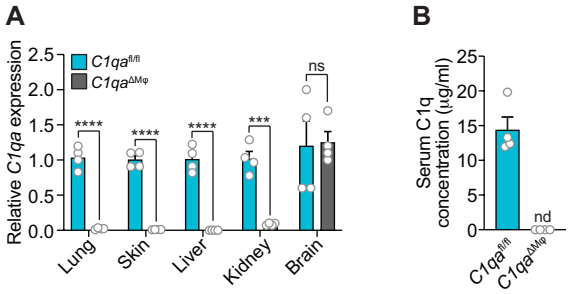

Figure 2 - figure supplement 1. C1q expression is lost systemically but preserved in the central nervous system of *C1qa*$^{\Delta M\varphi}$ mice.

(A) qPCR measurement of *C1qa* expression in lung, skin, liver, kidney, and brain. Each data point represents one mouse. Data are representative of two independent experiments.

(B) C1q is absent from the serum of *C1qa*$^{\Delta M\varphi}$ mice. Enzyme-linked immunosorbent assay (ELISA) detection of serum C1q protein from *C1qa*$^{fl/fl}$ and *C1qa*$^{\Delta M\varphi}$ littermates. Data are presented as C1q serum concentration based on a standard curve generated from purified recombinant mouse C1q. Each data point represents one mouse. nd, not detected. Data are representative of three independent experiments.

Error bars represent SEM. ***p<0.001; ****p<0.0001; ns, not significant by two-tailed Student's t-test.

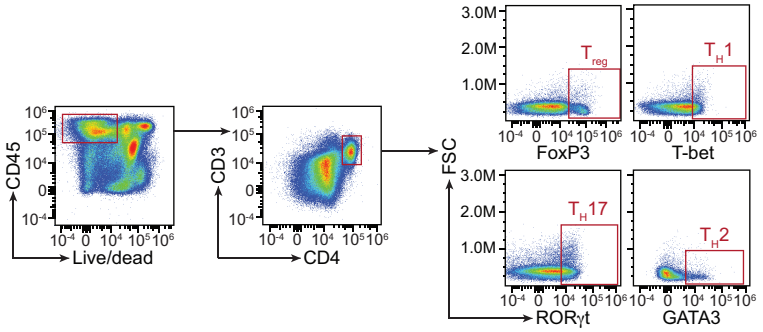

Figure 3 - figure supplement 1. Flow cytometry gating strategy for comparison of T cell populations in *C1qa*$^{fl/fl}$ and *C1qa*$^{\Delta M\varphi}$ mice.

Small intestinal cells were recovered from *C1qa*$^{fl/fl}$ and *C1qa*$^{\Delta M\varphi}$ littermates and analyzed by flow cytometry. T cells were gated as live CD45$^+$ CD3$^+$ CD4$^+$. T cell subsets were further identified by gating into T_{reg} (FoxP3$^+$), T_H1 (T-bet$^+$), T_H17 (RORγt$^+$), and T_H2 (GATA3$^+$). Representative plots from *C1qa*$^{fl/fl}$ mice are presented and comparisons between *C1qa*$^{fl/fl}$ and *C1qa*$^{\Delta M\varphi}$ littermates are shown in Figure 3. FSC, forward scatter.

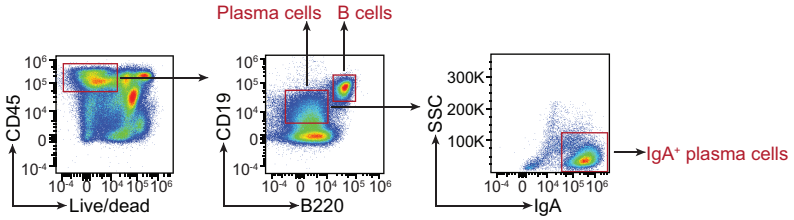

Figure 3 - figure supplement 2. Flow cytometry gating strategy for comparison of B cell and plasma cell populations in *C1qa*$^{fl/fl}$ and *C1qa*$^{\Delta M\varphi}$ mice.

Small intestinal cells were recovered from *C1qa*$^{fl/fl}$ and *C1qa*$^{\Delta M\varphi}$ littermates and analyzed by flow cytometry. B cells were gated as live CD45^{+} CD19^{+} B220^{+}. Plasma cells were gated as CD19^{+} B220^{-}, and IgA^{+} plasma cells were further identified. Representative plots from *C1qa*$^{fl/fl}$ mice are presented and comparisons between *C1qa*$^{fl/fl}$ and *C1qa*$^{\Delta M\varphi}$ littermates are shown in Figure 3. SSC, side scatter.

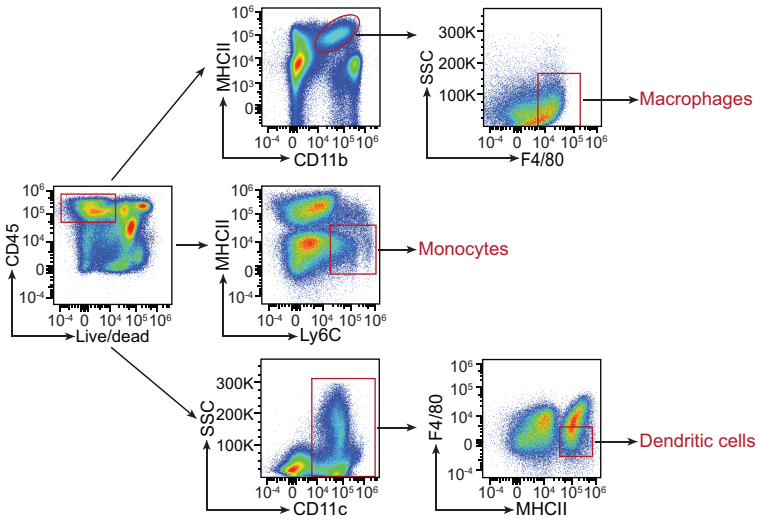

Figure 3 - figure supplement 3. Flow cytometry gating strategy for comparison of myeloid cell populations in *C1qa*$^{fl/fl}$ and *C1qa*$^{\Delta M\varphi}$ mice.

Small intestinal cells were recovered from *C1qa*$^{fl/fl}$ and *C1qa*$^{\Delta M\varphi}$ littermates and analyzed by flow cytometry. Macrophages were gated as live CD45^{+} MHCII^{+} CD11b^{+} F4/80^{hi}. Monocytes were gated as live CD45^{+} MHCII^{-} Ly6C$^{+.}$ Dendritic cells were gated as live CD45^{+} CD11c^{+} MHCII^{+} F4/80^{lo}. Representative plots from *C1qa*$^{fl/fl}$ mice are presented and comparisons between *C1qa*$^{fl/fl}$ and *C1qa*$^{\Delta M\varphi}$ littermates are shown in Figure 3. SSC, side scatter; MHCII, major histocompatibility complex II.

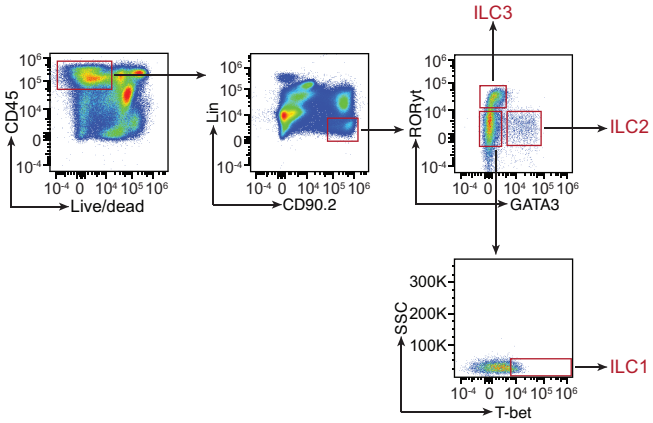

Figure 3 - figure supplement 4. Flow cytometry gating strategy for comparison of innate lymphoid cell populations in *C1qa*$^{fl/fl}$ and *C1qa*$^{\Delta M\varphi}$ mice.

Small intestinal cells were recovered from *C1qa*$^{fl/fl}$ and *C1qa*$^{\Delta M\varphi}$ littermates and analyzed by flow cytometry. Innate lymphoid cells (ILC) were gated as live CD45^{+} Lin^{-} CD90.2^{+} and then further identified as ILC1 (RORγt- GATA3^{-} T-bet^{+}), ILC2 (RORγt^{-} GATA3^{+}) and ILC3 (RORγt^{+} GATA3^{-}). Representative plots from *C1qa*$^{fl/fl}$ mice are presented and comparisons between *C1qa*$^{fl/fl}$ and *C1qa*$^{\Delta M\varphi}$ littermates are shown in Figure 3. SSC, side scatter.

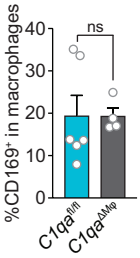

Figure 4 - figure supplement 1. Similar numbers of CD169^{+} macrophages are present in the small intestines of *C1qa*$^{\Delta M\varphi}$ and *C1qa*$^{fl/fl}$ littermates.

Flow cytometry analysis of CD169^{+} macrophages was conducted on cells recovered from the small intestines of *C1qa*$^{\Delta M\varphi}$ and *C1qa*$^{fl/fl}$ littermates. CD169^{+} cells were determined as a percentage of total macrophages (live CD45^{+} CD11b^{+} MHCII^{+} F4/80^{hi} cells).

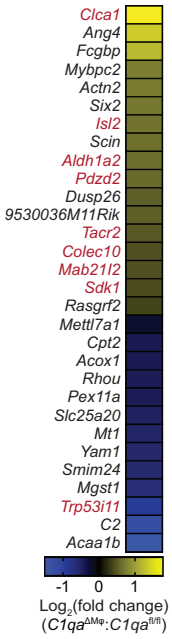

Figure 4 - figure supplement 2. The colonic longitudinal muscle myenteric plexus of *C1qa*$^{\Delta M\varphi}$ mice has a transcriptional profile similar to that of mice with a gastrointestinal motility disorder.
RNA-seq was performed on the colonic longitudinal muscle-myenteric plexus from five *C1qa*$^{fl/fl}$ and five *C1qa*$^{\Delta M\varphi}$ littermates. Genes that were differentially expressed are represented in a heatmap that depicts $\log_2$(fold change). Genes that also showed altered expression in the TashT mouse line, which is a model of human Hirschsprung's disease (Bergeron et al., 2015), are indicated in red. Statistical significance of overlap between differentially expressed genes in *C1qa*$^{\Delta M\varphi}$ and TashT mice was determined by Fisher's exact test ($p = 0.0032$).

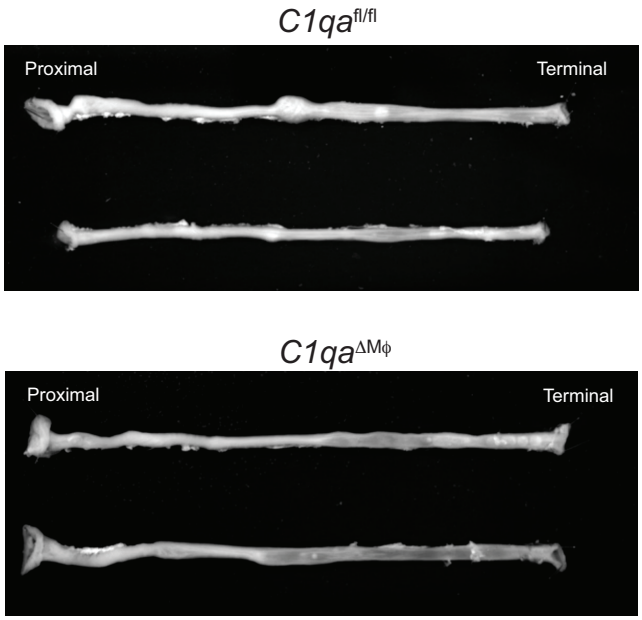

Figure 5 - figure supplements 1 and 2. *Ex vivo* video recordings of colonic peristalsis in *C1qa*$^{fl/fl}$ and *C1qa*$^{\Delta M\varphi}$ littermates.
Still images captured from *ex vivo* video recordings of colonic peristalsis to indicate orientation of the colons. Colons were allowed to equilibrate to the organ chamber for 30 minutes before video recording. Movies were captured over 15 minutes. Colons from *C1qa*$^{fl/fl}$ mice are shown in figure supplement 1; colons from *C1qa*$^{\Delta M\varphi}$ are shown in figure supplement 2.